

Weak precipitation, warm winters and springs impact glaciers of south slopes of Mt. Everest (central Himalaya) in the last two decades (1994-2013)

Franco Salerno^(1,4*), Nicolas Guyennon⁽²⁾, Sudeep Thakuri^(1,4), Gaetano Viviano⁽¹⁾, Emanuele Romano⁽²⁾, Elisa Vuillermoz⁽⁴⁾, Paolo Cristofanelli^(3,4), Paolo Stocchi⁽³⁾, Giacomo Agrillo⁽³⁾, Yaoming Ma⁽⁵⁾, Gianni Tartari^(1,4)

⁽¹⁾ National Research Council, Water Research Institute, Brugherio (IRSA -CNR), Italy

⁽²⁾ National Research Council, Water Research Institute, Roma (IRSA-CNR), Italy

⁽³⁾ National Research Council, Institute of Atmospheric Sciences and Climate (ISAC-CNR) Bologna, Italy

⁽⁴⁾ Ev-K2-CNR Committee, Via San Bernardino, 145, Bergamo 24126, Italy

⁽⁵⁾ Institute of Tibetan Plateau Research, Chinese Academy of Science, China

*Correspondence to Franco Salerno

Email: salerno@irsa.cnr.it

Address: IRSA-CNR Via Del Mulino 19. Località Occhiate 20861Brugherio (MB)

Phone: +39 039 21694221

Fax: +39 039 2004692

Abstract

Studies on recent climate trends from the Himalayan range are limited, and even completely absent at high elevation (> 5000 m a.s.l.). This contribution specifically explores the southern slopes of Mt. Everest (central Himalaya), analyzing the minimum, maximum, and mean temperature and precipitation time series reconstructed from seven stations located between 2660 and 5600 m a.s.l. over the last twenty years (1994-2013). We complete this analysis with data from all the existing ground weather stations located on both sides of the mountain range (Koshi Basin) over the same period. Overall we observe that the main and more significant increase in temperature is concentrated outside of the monsoon period. ~~At higher elevations~~ Above 5000 m a.s.l. minimum temperature ($\pm 0.072 \pm 0.011$ °C $\text{a}^+ \text{y}^{-1}$, $p < 0.001$) increased far more than maximum temperature ($\pm 0.009 \pm 0.012$ °C $\text{a}^- \text{y}^{-1}$, $p > 0.1$), while mean temperature increased by $\pm 0.044 \pm 0.008$ °C $\text{a}^+ \text{y}^{-1}$, $p < 0.05$. Moreover, we note a substantial liquid precipitation weakening (-9.3 ± 1.8 mm $\text{a}^+ \text{y}^{-1}$, $p < 0.01$ during the monsoon season). The annual rate of decrease in precipitation at higher elevation is similar to the one at lower altitudes on the southern side of the Koshi Basin, but ~~here~~ the drier conditions of this remote environment make the fractional loss much more consistent (-47% during the monsoon period). This study contributes to change the perspective on which climatic driver (temperature vs. precipitation) led mainly the glacier responses in the last twenty years. The main implications are the following: 1) the negative mass balances of glaciers

38 | observed in this region can be more ascribed to less accumulation due to weaker **solid**
39 precipitation than to an increase of melting processes. 2) The melting processes have
40 only been favored during winter and spring months and close to the glaciers terminus.
41 3) A decreasing of the probability of snowfall has significantly interested only the
42 | glaciers ablation zones (-10% , $p < 0.05$), but the magnitude of this phenomenon is
43 decidedly lower than the observed decrease of precipitation. 4) The lesser accumulation
44 could be the cause behind the observed lower glacier flow velocity and the current
45 stagnation condition of tongues, which in turn could have triggered melting processes
46 under the debris glacier coverage, leading to the formation of numerous supraglacial
47 and proglacial lakes that have characterized the region in the last decades. Without
48 demonstrating the causes that could have led to the climate change pattern observed at
49 | high elevation, we conclude -by listing the recent literature on hypotheses that accord
50 with our observations.

51 **Keywords:** temperature lapse rate, precipitation gradient, monsoon weakening,
52 Sequential Mann-Kendall, expectation maximization algorithm, climate change, glaciers
53 shrinkage, central Himalaya

54 **1 Introduction**

55 The current uncertainties concerning the glacial shrinkage in the Himalayas are
56 mainly attributed to a lack of measurements, both of the glaciers and of climatic forcing
57 agents (e.g., Bolch et al., 2012). Recent results underline the need for a fine scale inves-
58 tigation, especially at high altitude, to better model the hydrological dynamics in this ar-
59 ea. However, there are few high elevation weather stations in the world where the glaci-
60 ers are located (Tartari et al., 2009). This can be attributed to the remote location of
61 glaciers, the rugged terrain, and a complex political situation, all of which make phys-
62 ical access difficult (Bolch et al., 2012). As a consequence of the remoteness and diffi-
63 culty in accessing many high elevation sites combined with the complications of operat-
64 ing automated weather stations (AWSs) at these altitudes, long-term measurements are
65 challenging (Vuille, 2011). However, nearly all global climate models report increased
66 sensitivity to warming at high elevations (e.g., Rangwala and Miller, 2012), while ob-
67 servations are less clear (Pepin and Lundquist, 2008). Moreover, changes in the timing or
68 amount of precipitation are much more ambiguous and difficult to detect, and there is
69 no clear evidence of significant changes in total precipitation patterns in most mountain
70 regions (Vuille, 2011).

71 The need for a fine scale investigation is particularly evident on the south slope of
72 Mt. Everest (central Southern Himalaya, CH-S) as it is one of the heavily glaciated parts
73 of the Himalaya (Salerno et al., 2012; Thakuri et al., 2014). Nevertheless, these glaciers
74 have the potential to build up moraine-dammed lakes storing large quantities of water,
75 which are susceptible to GLOFs (glacial lake outburst floods) (e.g., Salerno et al., 2012;
76 Fujita et al., 2013). Gardelle et al. (2011) noted that this region is most characterized by
77 glacial lakes in the Hindu Kush Karakorum Himalaya. Recently, Thakuri et al. (2014)

78 noted that the Mt. Everest glaciers experienced an accelerated shrinkage in the last
79 twenty years (1992-2011), as underlined by an upward shift of the Snow Line Altitude
80 (SLA) with a velocity almost three times greater than the previous period (1962-1992).
81 Furthermore Bolch et al. (2011) and Nuimura et al. (2012) found a higher mass loss rate
82 during the last decade (2000–2010). Anyway, to date, there are not continuous
83 meteorological time series able to clarify the causes of the melting process to which the
84 glaciers of these slopes are subjected.

85 In this context, since the early 1990s, PYRAMID Observatory Laboratory (5050 m
86 [a.s.l.](#)) was created by the *Ev-K2-CNR Committee* (www.ev2cnr.org). This observatory
87 is located at the highest elevation at which weather data has ever been collected in the
88 region and thus represents a valuable dataset with which to investigate the climate
89 change in CH-S (Tartari et al., 2002; Lami et al., 2010). However, the remoteness and
90 the harsh conditions of the region over the years have complicated the operations of the
91 AWSs, obstructing long-term measurements from a unique station.

92 In this paper, we mainly explore the small scale climate variability of the south
93 slopes of Mt. Everest by analyzing the minimum, maximum, and mean air temperature
94 (T) and [liquid](#) precipitation (Prec) time series reconstructed from seven AWSs located
95 from 2660 to 5600 m a.s.l. over the last couple of decades (1994-2013). Moreover, we
96 complete this analysis with all existing weather stations located on both sides of the
97 Himalayan range (Koshi Basin) for the same period. In general, this study has the
98 ultimate goal of linking the climate change patterns observed at high elevation with the
99 glacier responses over the last twenty years, during which a more rapid glacier
100 shrinkage process occurred in the region of investigation.

101 **2 Region of investigation**

102 The current study is focused on the Koshi (KO) Basin which is located in the eastern
103 part of central Himalaya (CH) (Yao et al., 2012; Thakuri et al., 2014). To explore
104 possible differences in the surroundings of Mt. Everest, we decided to consider the
105 north and south parts of CH (with the suffixes -N and -S, respectively) separately (Fig.
106 1a). The KO River (58,100 km² of the basin) originates in the Tibetan Plateau (TP) and
107 the Nepali highlands. The area considered in this study is within the latitudes of 27° and
108 28.5° N and longitudes of 85.5° and 88° E. The altitudinal gradient of this basin is the
109 highest in the world, ranging from 77 to 8848 m a.s.l., i.e., Mt. Everest. We subdivide
110 the KO Basin into the northern side (KO-N), belonging to the CH-N, and southern side
111 (KO-S), belonging to the CH-S. The southern slopes of Mt. Everest are part of the
112 Sagarmatha (Everest) National Park (SNP) (Fig. 1b), where the small scale climate
113 variability at high elevation is investigated. The SNP is the world's highest protected
114 area, with over 30000 tourists in 2008 (Salerno et al., 2010a; Salerno et al., 2013). The
115 park area (1148 km²), extending from an elevation of 2845 to 8848 m a.s.l., covers the
116 upper Dudh Koshi (DK) Basin (Manfredi et al., 2010; Amatya et al., 2010). Land cover
117 classification shows that almost one-third of the territory is characterized by glaciers
118 and ice cover (Salerno et al., 2008; Tartari et al., 2008), while less than 10% of the park

119 area is forested (Bajracharya et al., 2010; Salerno et al., 2010b). The SNP presents a
120 broad range of bioclimatic conditions with three main bioclimatic zones: the zone of
121 alpine scrub; the upper alpine zone, which includes the upper limit of vegetation
122 growth; and the Arctic zone, where no plants can grow (UNEP and WCMC, 2008).
123 Figure 1c shows the glacier distribution along the hypsometric curve of the SNP. We
124 observe that the glacier surfaces are distributed from 4300 m to above 8000 m a.s.l.,
125 with more than 75% of the glacier surfaces lying between 5000 m and 6500 m a.s.l. The
126 2011 area-weighted mean elevation of the glaciers was 5720 m a.s.l. (Thakuri et al.,
127 2014). These glaciers are identified as the summer accumulation-type fed mainly by
128 summer Prec from the South Asian monsoon system, whereas the winter Prec caused by
129 the mid-latitude westerly wind is minimal (Yao et al., 2012). The prevailing direction of
130 the monsoons is S-N and SW-NE (e.g., Ichiyanagi et al., 2007). The climate is
131 influenced by the monsoon system because the area is located in the subtropical zone
132 with nearly 90% of the annual Prec falling in the months of June to September (this
133 study). Heavy autumn and winter snowfalls can occur in association with tropical
134 cyclones and westerly disturbances, respectively, and snow accumulation can occur at
135 high elevations at all times of the year (Benn, 2012). Bollasina et al. (2002) have
136 demonstrated the presence of well-defined local circulatory systems in the Khumbu
137 Valley (SNP). The local circulation is dominated by a system of mountain and valley
138 breezes. The valley breeze blows (approximately 4 m s^{-1}) from the south every day from
139 sunrise to sunset throughout the monsoon season, pushing the clouds that bring Prec
140 northward.

141 3 Data

142 3.1 Weather stations at high elevation

143 The first automatic weather station (named hereafter AWS0) at 5050 m a.s.l. near
144 | PYRAMID Observatory Laboratory (Fig. 1c), ~~and beginning was established~~ in October
145 | 1993, it has run continuously all year round (Bertolani et al., 2000). The station, operat-
146 | ing in extreme conditions, had recorded long-term ground-based ~~meteorological tem-~~
147 | ~~perature and temperature~~ data, ~~and the data- which~~ are considered valid until December
148 | 2005. Due to the obsolescence of technology, the station was disposed of in 2006. A
149 | new station (named hereafter AWS1) was installed just a few tens of meters away from
150 | AWS0 and has been operating since October 2000. Other stations were installed in the
151 | following years in the upper DK Basin in the Khumbu Valley (Table 1). In 2008, the
152 | network included ~~the~~ sixth monitoring points, ~~including~~ the highest weather station of
153 | the world, located at South Col of Mt. Everest (7986 m a.s.l.). The locations of all sta-
154 | tions are presented in Figure 1b. We can observe in Figure 1c that this meteorological
155 | network ~~represents well the climatic conditions~~ ~~represents the climatic conditions~~ of the
156 | SNP glaciers ~~well~~: AWS0 and AWS1 (5035 m a.s.l.) characterize the glacier fronts
157 | (4870 m a.s.l.), AWS4 (5600 m a.s.l.) represents the mean elevation of glaciers ~~in the~~

158 | [area](#) (5720 m a.s.l.), and AWS5, the surface station at South Col (7986 m a.s.l.), charac-
159 | terizes the highest peaks (8848 m a.s.l.).

160 | All stations, except AWS5 ([only T](#)), record at least T and Prec. This dataset presents
161 | some gaps (listed in Table 1) as a consequence of the complications of operating AWS
162 | at these altitudes. The list of measured variables for each stations and relevant data can
163 | be downloaded from <http://geonetwork.evk2cnr.org/>. Data processing and quality
164 | checks are performed according to the international standards of the WMO (World Me-
165 | teorological Organization).

166 | The Prec sensors at these locations are [conventional heated](#) tipping buckets ~~usually~~
167 | ~~used for rainfall measurements and which~~ may not fully capture the solid Prec. There-
168 | fore, [solid](#) Prec is probably underestimated, especially in winter. [However, in order to](#)
169 | [know the magnitude of the possible underestimation of the solid phase, we compared](#)
170 | [the monthly mean Prec of the reconstructed PYRAMID series \(1994-2013 period\) with](#)
171 | [the Prec of a station located downstream at 2619 m a.s.l. \(Chaurikhark, ID 1202\), \(Fig.](#)
172 | [1b, Table 2\) which presents monthly mean temperature above 0 °C even during the win-](#)
173 | [ter and thus a high prevalence of liquid Prec also during these months. This comparison,](#)
174 | [supported by the elevated correlation existing between the monthly Prec of the two sta-](#)
175 | [tions, shown a slight underestimation of the PYRAMID snow \(about 3±1% of total an-](#)
176 | [nual precipitation registered at PYRAMID, see Supplementary material 3 for more de-](#)
177 | [tails\). Therefore, being much reduced the underestimation, we decided not to manipu-](#)
178 | [late data. However the trends hereafter reported are referred mainly to the liquid phase](#)
179 | [of Prec.](#) In this regard, according to both Fujita and Sakai, 2014 and field observations
180 | (Ueno et al., 1994), the precipitation phase has been taken into account assuming that
181 | the probability of snowfall and rainfall depends on mean daily [air](#) temperature, using [as](#)
182 | [thresholds](#) – as proposed by the aforementioned authors – ~~as thresholds~~ 0 °C and 4 °C,
183 | respectively. In Figure 2 we first of all observe that at 5050 m a.s.l. 90% of precipitation
184 | is concentrated during June-September and that the probability of snowfall is very low
185 | (4%), considering that the mean daily temperature during these months is above 0 °C.
186 | On a yearly basis, this probability reaches 20% of the annual cumulated precipitation.

187 | 3.2 Other weather stations at lower altitude in the Koshi Basin

188 | In KO-S Basin (Nepal), the stations are operated by the Department of Hydrology
189 | and Meteorology (DHM) (www.dhm.gov.np/). For daily T and Prec, we selected 10
190 | stations for T and 19 stations for Prec considering both the length of the series and the
191 | monitoring continuity (< 10% of missing daily data). The selected stations cover an
192 | elevation range between 158 and 2619 m a.s.l. (Table 3). In KO-N Basin (TP, China),
193 | the number of ground weather stations (operated by the Chinese Academy of Science
194 | (CAS)), selected with the same criteria mentioned above, is considerably smaller, just
195 | two, but these stations have a higher elevation (4302 m [a.s.l.](#) for the Dingri station and
196 | 3811 m a.s.l. for the Nyalam station).

197 | [The quality insurance of these meteorological data is ensured considering that they](#)

198 | [are used as part of global and regional networks including for instance APHRODITE](#)
199 | [\(Asian Precipitation–Highly Resolved Observational Data Integration Towards](#)
200 | [Evaluation of Water Resources\) \(Yasutomi et al., 2011\) and GHCN \(Global Historical](#)
201 | [Climatology Network\) \(Menne et al., 2012\).](#)

202 | **4 Methods**

203 | We define the pre-monsoon, monsoon, and post-monsoon seasons as the months
204 | from February to May, June to September, and October to January, respectively. The
205 | minT, maxT, and meanT are calculated as the minimum, maximum, and mean daily air
206 | temperature. For total precipitation (Prec), we calculate the mean of the cumulative
207 | precipitation for the analyzed period.

208 | 4.1 Reconstruction of the daily temperature and precipitation time series at high 209 | elevation

210 | The two stations named AWS0 and AWS1 in the last twenty years, considering the
211 | extreme weather conditions of ~~these slopes~~[this area](#), present a percentage of missing
212 | daily values of approximately 20% (Table 1). The other stations (hereafter named
213 | secondary stations) were used here for infilling the gaps according to a priority criteria
214 | based on the degree of correlation among data. AWS1 was chosen as the reference
215 | station given the length of the time series and that it is currently still operating.
216 | Therefore, our reconstruction (hereafter named PYRAMID) is referred to an elevation
217 | of 5035 m a.s.l.

218 | The selected infilling method is a simple regression analysis based on quantile
219 | mapping (e.g., Déqué, 2007; Themeßl et al., 2012). This ~~simple~~ regression method has
220 | been preferred to more complex techniques, such as the fuzzy rule-based approach
221 | (Abebe et al., 2000) or the artificial neural networks (Abudu et al., 2010; Coulibaly and
222 | Evora, 2007), considering the peculiarity of this case study. In fact, all stations are
223 | located in the same valley (Khumbu Valley). This aspect confines the variance among
224 | the stations to the altitudinal gradient of the considered variable (T or Prec), which can
225 | be easily reproduced by the stochastic link created by the quantile mapping method. In
226 | case all stations registered a simultaneous gap, we apply a multiple imputation
227 | technique (Schneider, 2001) that uses some other proxy variables to fill the remaining
228 | missing data. Details on the reconstruction procedure and the computation of the
229 | associated uncertainty are provided in Supplementary Material 1.

230 | 4.2 The trends analysis: the Sequential Mann-Kendall test

231 | The Mann-Kendall (MK) test (Kendall, 1975) is widely adopted to assess significant
232 | trends in hydro-meteorological time series (e.g., Carraro et al., 2012a, 2012b; Guyennon
233 | et al., 2013). This test is non-parametric, thus being less sensitive to extreme sample
234 | values, and is independent of the hypothesis about the nature of the trend, whether

235 linear or not. The MK test verifies the assumption of the stationarity of the investigated
236 series by ensuring that the associated normalized Kendall's tau coefficient, $\mu(\tau)$, is
237 included within the confidence interval for a given significance level (for $\alpha = 5\%$, the
238 $\mu(\tau)$ is below -1.96 and above 1.96). In the sequential form (seqMK) (Gerstengarde
239 and Werner, 1999), $\mu(\tau)$ is calculated for each element of the sample. The procedure
240 is applied forward starting from the oldest values (progressive) and backward starting
241 from the most recent values (retrograde). If no trend is present, the patterns of
242 progressive and retrograde $\mu(\tau)$ versus time (i.e., years) present several crossing
243 points, while a unique crossing period allows the approximate location of the starting
244 point of the trend (e.g., Bocchiola and Diolaiuti, 2010).

245 In this study, the seqMK is applied to monthly vectors. Monitoring the seasonal non-
246 stationarity, the monthly progressive $\mu(\tau)$ is reported with a pseudo color code, where
247 the warm colors represent the positive slopes and cold colors the negative ones. Color
248 codes associated with values outside of the range (-1.96 to 1.96) possess darker tones to
249 highlight the trend significance (Salerno et al., 2014). Moreover, to monitor the overall
250 non-stationarity of the time series, both the progressive and the retrograde $\mu(\tau)$ at the
251 annual scale are reported. We used the Sen's slope proposed by Sen (1968) as a robust
252 linear regression allowing the quantification of the potential trends revealed by the
253 seqMK (e.g., Bocchiola and Diolaiuti, 2010). The significance level is established for p
254 < 0.05 . We define a slight significance for $p < 0.10$. The uncertainty associated with the
255 Sen's slopes (1994-2013) is estimated through a Monte Carlo uncertainty analysis (e.g.,
256 James and Oldenburg, 1997), described in detail in Supplementary Material 1.

257 5 Results

258 5.1 Trend analysis at high elevation

259 Figure 3 shows the reconstructed PYRAMID time series for minT, maxT, meanT,
260 and Prec resulting from the overall infilling process explained in Supplementary
261 Material 1. Figure 4 analyzes the monthly trends of T and Prec from 1994 to 2013 for
262 PYRAMID.

263 *Minimum air temperature (minT)*

264 | November (± 0.17 °C $\mathbf{a^+ y^{-1}}$, $p < 0.01$) and December (± 0.21 °C $\mathbf{a^+ y^{-1}}$, $p < 0.01$)
265 present the highest increasing trend, i.e., both these two months experienced about even
266 $+4$ °C over twenty years (Fig. 4a). In general, the post- and pre-monsoon periods
267 experience higher and more significant increases than during the monsoon. In particular,
268 | we note the significant and consistent increase of minT of April (± 0.10 °C $\mathbf{a^+ y^{-1}}$, $p <$
269 0.05). At the annual scale, the bottom graph shows a progressive $\mu(\tau)$ trend parallel to
270 the retrograde $\mu(\tau)$ one for the entire analyzed period, i.e., a continuous tendency of
271 minT to rise, which becomes significant in 2007, when the progressive $\mu(\tau)$ assumes
272 values above $+1.96$. On the right, the Sen's slope completes the analysis, illustrating that

273 | minT is increasing at annual level by $\pm 0.072 \pm 0.011 \text{ } ^\circ\text{C a}^+ \text{ y}^{-1}$, $p < 0.001$, i.e., $+1.44 \pm$
274 | $0.22 \text{ } ^\circ\text{C}$ over twenty years.

275 | *Maximum air temperature (maxT)*

276 | The post- and pre-monsoon months show larger increases in maxT, but with lower
277 | magnitudes and significance than we observe for minT (Fig. 4b). The highest increases
278 | for this variable occurs also for ~~this variable~~ maxT in April, November and December.
279 | Less expected is the decrease of maxT in May ($-0.08 \text{ } ^\circ\text{C a}^+ \text{ y}^{-1}$, $p < 0.05$) and during the
280 | monsoon months from June to August ($-0.05 \text{ } ^\circ\text{C a}^+ \text{ y}^{-1}$, $p < 0.1$). On the annual scale,
281 | the bottom graph shows a continuous crossing of the progressive and retrograde $\mu(\tau)$
282 | trends until 2007, i.e., a general stationary condition. From 2007 until 2010, the trend
283 | significantly increased, while 2012 and 2013 register a decrease, bringing the
284 | progressive $\mu(\tau)$ near the stationary condition. In fact, on the right, the Sen's slope
285 | confirms that maxT is at annual level stationary over the twenty years ($+0.009 \pm 0.012$
286 | $^\circ\text{C a}^+ \text{ y}^{-1}$, $p > 0.1$).

287 | *Mean air temperature (meanT)*

288 | Figure 4c, as expected, presents intermediate conditions for meanT ~~than in respect to~~
289 | ~~for~~ minT and maxT. All months, except May and the monsoon months from June and
290 | August, register a positive trend (more or less significant). December presents the
291 | highest a more significant increasing trend ($\pm 0.17 \text{ } ^\circ\text{C a}^+ \text{ y}^{-1}$, $p < 0.01$), while April
292 | shows the highest and a more significant increase ($p < 0.10$) during the pre-monsoon
293 | period. On the annual scale, the bottom graph shows that the progressive $\mu(\tau)$ trend
294 | has always increased since 2000 and that it becomes significant beginning in 2008. On
295 | the right, the Sen's slope concludes this analysis, showing that meanT has been
296 | significantly increasing by $\pm 0.044 \pm 0.008 \text{ } ^\circ\text{C a}^+ \text{ y}^{-1}$, $p < 0.05$, i.e., $+0.88 \pm 0.16 \text{ } ^\circ\text{C}$ over
297 | twenty years.

298 | *Total precipitation (Prec)*

299 | In the last years, all cells are blue, i.e., we observe for all months an overall and
300 | strongly significant decreasing trend of Prec (Fig. 4d). In general, the post- and pre-
301 | monsoon periods experience more significant decreases, although the monsoon months
302 | (June-September) register the main Prec losses (e.g. August registers a Prec loss of even
303 | $-4.6 \text{ mm a}^+ \text{ y}^{-1}$). On the annual scale, the bottom graph shows a continuous decreasing
304 | progressive $\mu(\tau)$ trend since 2000 that becomes significant beginning in 2005. On the
305 | right, the Sen's slope notes that the decreasing Prec trend is strongly high and
306 | significant at annual level ($-13.7 \pm 2.4 \text{ mm a}^+ \text{ y}^{-1}$, $p < 0.001$).

307 | The precipitation reduction is mainly due to a reduction in intensity (cumulative
308 | precipitation for week). However during the early and late monsoon rather show a
309 | reduction in duration (number of we days for week) (see further details in
310 | Supplementary Material 2).

311 5.2 Trend analysis in the Koshi Basin

312 Table 2 provides the descriptive statistics of the Sen's slopes for minT, maxT,
313 meanT, and Prec for the 1994-2013 period for the Koshi Basin. The stations located on
314 the two sides of the Himalayan range are listed separately. For the southern ones (KO-
315 S), we observe that for minT less than half of the stations experience an increasing trend
316 and just three are significant with $p < 0.1$. In general, the minT on the southern side can
317 be defined as stationary ($+0.003 \text{ } ^\circ\text{C } \underline{\mathbf{a}^+ \mathbf{y}^{-1}}$). Conversely, the maxT shows a decidedly
318 non-stationary condition. All stations present an increasing trend, and even six of the ten
319 are on the significant rise with at least $p < 0.1$. The mean trend is $+0.060 \text{ } ^\circ\text{C } \underline{\mathbf{a}^+ \mathbf{y}^{-1}}$ ($p <$
320 0.10). Similarly, the meanT shows a substantial increase. Also in this case, six of the ten
321 stations are on the significant rise with at least $p < 0.1$. The mean trend is $+0.029 \text{ } ^\circ\text{C } \underline{\mathbf{a}^+ \mathbf{y}^{-1}}$
322 ($p < 0.10$). In regards to Prec, we observe that on the KO-S, 14 of the 19 stations
323 present a downward trend. Among them, eight decrease significantly with at least $p <$
324 0.1 . The mean trend is $-11.1 \text{ mm } \underline{\mathbf{a}^+ \mathbf{y}^{-1}}$, i.e., we observe a decreasing of 15% (222 mm)
325 of precipitation fallen in the basin during the 1994-2013 period (1527 mm on average).

326 The two stations located on the northern ridge (KO-N) show a singularly slight sig-
327 nificant rise for minT ($\underline{+0.034 \text{ } ^\circ\text{C } \mathbf{a}^+ \mathbf{y}^{-1}}$, $p < 0.10$ on average) and for maxT ($\underline{+0.039 \text{ } ^\circ\text{C}}$
328 $\underline{\mathbf{a}^+ \mathbf{y}^{-1}}$, $p < 0.10$ on average), recording a consequent mean increase of meanT equal to
329 $\underline{+0.037 \text{ } ^\circ\text{C } \mathbf{a}^+ \mathbf{y}^{-1}}$, $p < 0.05$. As for Prec, we observe that on the KO-N both stations
330 maintain stationary conditions ($-0.1 \text{ mm } \underline{\mathbf{a}^+ \mathbf{y}^{-1}}$).

331 Table 3 provides the descriptive statistics of the Sen's slopes on a seasonal base. The
332 stations analyzed here are the same as those considered in Table 2. We begin our
333 description with PYRAMID, already analyzed in detail in Figure 4. We confirm with
334 this seasonal grouping that the main and significant increases of minT, maxT, and
335 meanT are completely concentrated during the post-monsoon period (e.g., $\underline{+0.124 \text{ } ^\circ\text{C } \mathbf{a}^-}$
336 $\underline{\mathbf{y}^{-1}}$, $p < 0.01$ for meanT). The pre-monsoon period experienced a slighter and not
337 significant increase (e.g., $\underline{+0.035 \text{ } ^\circ\text{C } \mathbf{y}^{-1}}$, $p > 0.1$ for meanT). In general, during the
338 monsoon period, T is much more stationary for all three variables (e.g., $\underline{+0.015 \text{ } ^\circ\text{C } \mathbf{y}^{-1}}$, p
339 > 0.1 for meanT). Considering the other KO-S stations, the main increasing and
340 significant trends of meanT occurred during the pre-monsoon ($\underline{+0.043 \text{ } ^\circ\text{C } \mathbf{a}^+ \mathbf{y}^{-1}}$) and
341 post-monsoon ($\underline{+0.030 \text{ } ^\circ\text{C } \mathbf{a}^+ \mathbf{y}^{-1}}$) season, while the increase during the monsoon is
342 slighter ($\underline{+0.020 \text{ } ^\circ\text{C } \mathbf{a}^+ \mathbf{y}^{-1}}$). The KO-N stations confirm that the main increasing trend of
343 meanT occurred outside the monsoon period that is stationary ($+0.013 \text{ } ^\circ\text{C } \underline{\mathbf{a}^+ \mathbf{y}^{-1}}$).

344 As for Prec, PYRAMID and the other KO-S stations show that the magnitude of the
345 Sen's slopes is higher during the monsoon season ($-9.3 \text{ mm } \underline{\mathbf{a}^+ \mathbf{y}^{-1}}$ and $-8.6 \text{ mm } \underline{\mathbf{a}^+ \mathbf{y}^{-1}}$,
346 respectively), when precipitation is more abundant. The relatively low snowfall phase of
347 monsoon Prec at PYRAMID (as specified above) makes the decreasing trend observed
348 during the summer more robust than the annual one as devoid of ~~possible the~~
349 undervaluation of snowfall, although slight as demonstrated above (3±1%). The
350 northern stations show slight significant decreasing Prec during the winter ($-3.3 \text{ mm } \underline{\mathbf{a}^-}$
351 $\underline{\mathbf{y}^{-1}}$, $p < 0.05$).

352 5.3 Lapse rates in the southern Koshi Basin

353 5.3.1 Air temperature gradient

354 This study, aiming to create a connection between the climate drivers and cryosphere
355 in the Koshi Basin, which presents the highest altitudinal gradient of the world (77 to
356 8848 m a.s.l.), offers a unique opportunity to calculate T and Prec lapse rates before
357 analyzing their spatial trends. It is worth noting that the T lapse rate is one of the most
358 important variables for modeling meltwater runoff from a glacierized basin using the T-
359 index method (Hock, 2005; Immerzeel et al., 2014). It is also an important variable for
360 determining the form of Prec and its distribution characteristics (e.g., Hock, 2005).
361 Figure 5a-5b presents the lapse rate of the annual mean T in the KO Basin (Nepal) along
362 the altitudinal range of well over 7000 m (865 to 7986 m a.s.l.). We found an altitudinal
363 gradient of $-0.60\text{ }^{\circ}\text{C (100 m)}^{-1}$ on the annual scale with a linear trend ($r^2 = 0.98$, $p <$
364 0.001). It is known that up to altitudes of approximately 8-17 km a.s.l. in the lower
365 regions of the atmosphere, T decreases with altitude at a fairly uniform rate (Washington
366 and Parkinson, 2005). ~~Kattel and Yao (2013) recently found a lower annual lapse rate~~
367 ~~for the overall CH-S, but until 4000 m a.s.l.: $-0.52\text{ }^{\circ}\text{C (100 m)}^{-1}$.~~

368 Considering that the lapse rate is mainly affected by the moisture content of the air
369 (Washington and Parkinson, 2005), we ~~also~~ calculated the seasonal gradients (not
370 shown here). We found a dry lapse rate of $-0.65\text{ }^{\circ}\text{C (100 m)}^{-1}$ ($r^2 = 0.99$, $p < 0.001$)
371 during the pre-monsoon season when AWS1 registers a mean relative humidity of 62%.
372 A saturated lapse rate during the monsoon season is $-0.57\text{ }^{\circ}\text{C (100 m)}^{-1}$ ($r^2 = 0.99$, $p <$
373 0.001) with a mean relative humidity of 96%. During the post-monsoon period, we
374 found a lapse rate equal to that registered during the monsoon: $-0.57\text{ (100 m)}^{-1}$ ($r^2 =$
375 0.98 , $p < 0.001$) even if the relative humidity is decidedly lower in these months (44%).
376 Kattel and Yao (2013) explain this anomalous low post-monsoon lapse rate as the effect
377 of strong radiative cooling in winter.

378 5.3.2 Precipitation gradient

379 ~~The relationship of Prec with elevation helps in As for Prec, its relationship with~~
380 ~~elevation helps in~~ providing a realistic assessment of water resources and hydrological
381 modeling of mountainous regions (Barros et al., 2004). In recent years, the spatial
382 variability of Prec has received attention because the mass losses of the Himalayan
383 glaciers can be explained with an increased variability in the monsoon system (e.g., Yao
384 et al., 2012; Thakuri et al., 2014). ~~Some previous studies of the Himalayas have~~
385 ~~considered orographic effects on Prec (Singh and Kumar, 1997; Ichiyonagi et al., 2007).~~
386 ~~Ichiyonagi et al. (2007), using all available Prec stations operated by DHM, of which~~
387 ~~5% of stations are located over 2500 m and just one station is over 4000 m a.s.l.,~~
388 ~~observed that in the CH-S region, the annual Prec increases with altitude below 2000 m~~
389 ~~a.s.l. and decreases for elevations ranging between 2000 and 3500 m a.s.l., but with no~~
390 ~~significant gradient. A broad picture of the relationship between Prec and topography in~~

391 ~~the Himalayas can be derived from the precipitation radar onboard the Tropical Rainfall~~
392 ~~Measuring Mission (TRMM). Some authors found an increasing trend with elevation~~
393 ~~characterized by two distinct maxima along two elevation bands (950 and 2100 m~~
394 ~~a.s.l.). The second maximum is much higher than the first, and it is located along the~~
395 ~~Lesser Himalayas. Over these elevations, the annual distribution follows an~~
396 ~~approximate exponentially decreasing trend (Bookhagen and Burbank, 2006).~~

397 Figure 5~~ab~~ shows the altitudinal gradient for the total annual Prec in the Koshi Basin.
398 We observe a clear rise in Prec with elevation until approximately 2500 m a.s.l.,
399 corresponding to the Tarke Ghyang station (code 1058), registering an annual mean of
400 3669 mm (mean for the 2004-2012 period). A linear approximation ($r = 0.83$, $p < 0.001$)
401 provides a rate of $+1.16 \text{ mm m}^{-1}$. At higher elevations, we observe an exponential
402 decrease (ae^{bx} , with $a = 21168 \text{ mm m}^{-1}$ and $b = -9 \cdot 10^{-4} \text{ m}^{-1}$, where x is the elevation
403 expressed as m a.s.l.) until observing a minimum of 132 mm (years 2009 and 2013) for
404 the Kala Patthar station (AWS4) at 5600 m a.s.l., although, as specified above, at these
405 altitudes the contribution of winter snowfall could be slightly underestimated. The
406 changing point between the two gradients can be reasonably assumed at approximately
407 2500 m a.s.l., considering that the stations here present the highest interannual
408 variability, belonging in this way, depending on the year, to the linear increase or to the
409 exponential decrease. The clear outlier along the linear gradient is the Num Station
410 (1301) located at 1497 m a.s.l., which recorded 4608 mm of precipitation. This station
411 has been excluded for the linear approximation because, as reported by Montgomery
412 and Stolar (2006), the station is located in the Arun Valley, which acts as a conduit for
413 northward transport of monsoonal precipitation. The result is that local precipitation
414 within the gorge of the Arun River is several times greater than in surrounding areas.

415 Some previous studies of the Himalayas have considered orographic effects on Prec
416 (Singh and Kumar, 1997; Ichiyanagi et al., 2007). Ichiyanagi et al. (2007), using all
417 available Prec stations operated by DHM, of which $< 5\%$ of stations are located over
418 2500 m and just one station is over 4000 m a.s.l., observed that in the CH-S region, the
419 annual Prec increases with altitude below 2000 m a.s.l. and decreases for elevations
420 ranging between 2000 and 3500 m a.s.l., but with no significant gradient. A broad
421 picture of the relationship between Prec and topography in the Himalayas can be
422 derived from the precipitation radar onboard the Tropical Rainfall Measuring Mission
423 (TRMM). Some authors found an increasing trend with elevation characterized by two
424 distinct maxima along two elevation bands (950 and 2100 m a.s.l.). The second
425 maximum is much higher than the first, and it is located along the Lesser Himalayas.
426 Over these elevations, the annual distribution follows an approximate exponentially
427 decreasing trend (Bookhagen and Burbank, 2006).

428 Physically, we can interpret the Prec gradient of Fig. 5a considering that when the
429 humid air masses coming from the Bay of Bengal collide with the orographic barrier,
430 heavy convections induce huge quantity of rain below 2500 m a.s.l.. The topographic
431 barrier of the Himalayan mountain range causes the mechanical lift of the humid air, the
432 cooling of the air column, the condensation and the consequent rainfall. The further

433 increase in relief induces a depletion of the moisture content resulting in a severe
434 reduction of Prec at higher altitudes. Our study, based on ground stations, confirms the
435 general Prec gradient detected with the TRMM microwave observations, even if we did
436 not identified a marked double maximum Prec peak as observed generally for the whole
437 central Himalaya by Bookhagen and Burbank, 2006. In fact these author report for our
438 specific case study (profiles 14 and 15 of their Fig.1(b)) a single step increase in relief
439 associated with a single Prec maximum.

440 5.4 Spatial distribution of air temperature and precipitation trends in the Koshi Basin

441 Figure 6 presents the spatial distribution of the Sen's slopes in the Koshi Basin for
442 minT (Fig. 6a), maxT (Fig. 6b), meanT (Fig. 6c), and Prec (Fig. 6d) during the 1994-
443 2013 period. The relevant data are reported in Table 2. The Chainpur (East) station
444 shows T trends in contrast with the other stations (see also Table 2); therefore, we
445 consider this station as a local anomaly and do not discuss it further in the following
446 sections.

447 In regards to minT, we observe an overall stationary condition in KO-S, as noted
448 above. The only two stations showing a significant increasing trend are both located at
449 East. The high elevation stations (PYRAMID and both those located on the north ridge)
450 differ from the general pattern of the southern basin by showing a significant increasing
451 trend. Even for maxT, we observe a higher increase in the southeastern basin. The
452 central and western parts of the KO-S seem to be more stationary. PYRAMID follows
453 this stationary pattern, while the northern stations (KO-N) show large and significant
454 increases. As a consequence, meanT shows increasing trends for all the Koshi Basin,
455 especially on the southeast and northern sides.

456 The decrease of precipitation in the southern Koshi Basin presents a quite
457 homogeneous pattern from which the highly elevated PYRAMID is not excluded. The
458 pattern is different on the north ridge, where it is stationary.

459 6 Discussion

460 6.1 Temperature trends of the Koshi Basin compared to the regional pattern

461 The trend analysis carried out in this study for the last two decades in KO-S shows
462 full consistency with the pattern of change (shown in the following) occurring in these
463 regions over the last three decades in terms of a higher increase in maxT (+0.060 °C y⁻¹)
464 than in minT (+0.003 °C y⁻¹), a seasonal pattern (more pronounced during the pre- and
465 post-monsoon months), and the magnitudes of the trends (e.g., the meanT trend is
466 +0.030 °C y⁻¹). Therefore, at low elevations of KO-S, we observe an acceleration of
467 warming in the recent years compared to the rate of change reported by Kattel and Yao
468 (2013) and Shrestha et al. (1999) in the previous decades.

469 At regional level, Kattel and Yao (2013) analyzed the annual minT, maxT, and
470 meanT trends from stations ranging from 1304 m to 2566 m a.s.l. in CH-S (correspond-
471 ing to all stations in Nepal) during the 1980–2009 period. They found that the magni-

472 | tude of warming is higher for maxT ($\pm 0.065 \text{ }^\circ\text{C a}^{-1}\text{y}^{-1}$), while minT ($\pm 0.011 \text{ }^\circ\text{C a}^{-1}\text{y}^{-1}$)
473 | exhibits larger variability, such as positive, negative or no change; meanT was found to
474 | increase at an intermediate rate of $\pm 0.038 \text{ }^\circ\text{C a}^{-1}\text{y}^{-1}$. These authors extended some time
475 | series and confirmed the findings of Shrestha et al. (1999) that, analyzing the 1971-1994
476 | period, found a maxT increase of $\pm 0.059 \text{ }^\circ\text{C a}^{-1}\text{y}^{-1}$ for all of Nepal. Furthermore, warm-
477 | ing in the winter was more pronounced compared to other seasons in both studies.
478 | These results are consistent with the pattern reported in WH (e.g., Bhutiyani et al.,
479 | 2007; Shekhar et al., 2010), in EH, and in the rest of India (e.g., Pal and Al-Tabbaa,
480 | 2010) for the last three decades.

481 | ~~The trend analysis carried out in this study for the last two decades in KO-S shows~~
482 | ~~full consistency with the pattern of change occurring in these regions over the last three~~
483 | ~~decades in terms of a higher increase in maxT ($0.060 \text{ }^\circ\text{C a}^{-1}$) than in minT ($0.003 \text{ }^\circ\text{C a}^{-1}$),~~
484 | ~~a seasonal pattern (more pronounced during the pre and post monsoon months), and~~
485 | ~~the magnitudes of the trends (e.g., the meanT trend is $+0.030 \text{ }^\circ\text{C a}^{-1}$). Therefore, at low~~
486 | ~~elevations of KO-S, we observe an acceleration of warming in the recent years com-~~
487 | ~~pared to the rate of change reported by Kattel and Yao (2013) and Shrestha et al. (1999)~~
488 | ~~in the previous decades.~~

489 | The trend analysis carried out in this study for the last two decades in KO-N agrees
490 | with the regional studies (shown in the following) in regards to both the considerable
491 | increase of minT ($+0.034 \text{ }^\circ\text{C y}^{-1}$) and the seasonal consistency of trends, related to all
492 | three T variables, outside the monsoon months. However, we observe that in recent
493 | years, maxT is increasing more than the rest of the TP ($+0.039 \text{ }^\circ\text{C y}^{-1}$). In general we
494 | observed an increase of meanT ($0.037 \text{ }^\circ\text{C y}^{-1}$) comparable to that reported by Yang et al.
495 | (2012) ($0.031 \text{ }^\circ\text{C y}^{-1}$) in the 1971-2007 period.

496 | ~~At regional level, Different conditions have been observed~~ on the TP, ~~where~~ the
497 | warming of minT is more prominent than that of maxT (e.g., Liu et al., 2006; Liu et al.,
498 | 2009). In particular, for stations above 2000 m a.s.l. during the 1961-2003 period, Liu
499 | et al. (2006) found that minT trends were consistently greater ($+0.041 \text{ }^\circ\text{C a}^{-1}\text{y}^{-1}$) than
500 | those of maxT ($+0.018 \text{ }^\circ\text{C a}^{-1}\text{y}^{-1}$), especially in the winter and spring months. Yang et al.
501 | (2012), focusing their analysis on CH-N (which corresponds to the southern TP) in a
502 | more recent period (1971-2007), showed a significant increase of $\pm 0.031 \text{ }^\circ\text{C a}^{-1}\text{y}^{-1}$ for
503 | meanT. Yang et al. (2006) analyzed five stations located in a more limited area of CH-
504 | N: the northern side of Mt. Everest (therefore, including the two stations also considered
505 | in this study) from 1971 to 2004. The warming is observed to be influenced more mark-
506 | edly by the minT increase.

507 | ~~The trend analysis carried out in this study for KO-N over the last two decades~~
508 | ~~agrees with these studies in regards to both the considerable increase of minT ($0.034 \text{ }^\circ\text{C}$~~
509 | ~~a^{-1}) and the seasonal consistency of trends, related to all three T variables, outside the~~
510 | ~~monsoon months. However, we observe that in recent years, maxT is increasing more~~
511 | ~~than the rest of the TP ($0.039 \text{ }^\circ\text{C a}^{-1}$). In general we observed an increase of meanT~~
512 | ~~($0.037 \text{ }^\circ\text{C a}^{-1}$) comparable to that reported by Yang et al. (2012) ($0.031 \text{ }^\circ\text{C a}^{-1}$) in the~~
513 | ~~1971-2007 period.~~

514 | ~~With all these regional studies,~~ Summarizing PYRAMID shares the higher T trends
515 | outside the monsoon period. However, in contrast with studies located south of the
516 | Himalayan ridge, which observed a prevalence of maxT increase, PYRAMID experi-
517 | enced a consistent minT increase (± 0.072 °C $\text{a}^{-1}\text{y}^{-1}$ for PYRAMID vs ± 0.003 °C $\text{a}^{-1}\text{y}^{-1}$
518 | for KO-S stations), while the maxT increase is decidedly weaker (± 0.009 °C $\text{a}^{-1}\text{y}^{-1}$ for
519 | PYRAMID vs ± 0.060 °C $\text{a}^{-1}\text{y}^{-1}$ for KO-S stations). The remarkable minT trend of
520 | PYRAMID is higher, but more similar to the pattern of change commonly described on
521 | the TP, in particular in CH-N, and also in this study (± 0.072 °C $\text{a}^{-1}\text{y}^{-1}$ for PYRAMID vs
522 | ± 0.034 °C $\text{a}^{-1}\text{y}^{-1}$ for KO-N stations), while the maxT increase is weaker (± 0.009 °C $\text{a}^{-1}\text{y}^{-1}$
523 | $\text{a}^{-1}\text{y}^{-1}$ for PYRAMID vs ± 0.039 °C $\text{a}^{-1}\text{y}^{-1}$ for KO-N stations).

524 | 6.2 Elevation dependency of temperature trends

525 | Figure 7 shows T trends in the KO Basin for minT, meanT, and maxT relative to the
526 | elevation during the 1994-2013 period. No linear pattern emerges. However, we can
527 | observe the minT trend of the three stations located at higher altitude (PYRAMID and
528 | KO-N stations), which increases more than that of the lower stations (Fig. 7a, see also
529 | Table 2). Reviewing the most recent studies in the surroundings, we found that they are
530 | quite exclusively located on CH-N. These studies often show contradictory elevation
531 | dependencies (Rangwala and Miller, 2012). A recent study by You et al. (2010) did not
532 | find any significant elevation dependency in the warming rates of meanT between 1961
533 | and 2005. However, considering mostly the same stations, Liu et al. (2009) found that
534 | the warming rates for minT were greater at higher elevations. Observations from CH-S
535 | are much rarer. Shrestha et al. (1999) found elevation dependency in the rate at which
536 | maxT were increasing in the Nepali Himalayas (CH-S), with higher rates at higher
537 | elevations, but this study exclusively considered stations under 3000 m a.s.l.

538 | Furthermore we did not find for the Koshi Basin any significant elevation
539 | dependency in the weakening rates of Prec.

540 | 6.3 Precipitation trends of the Koshi Basin compared to the regional pattern

541 | As will be detailed in the following, different from the north side of Mt. Everest and
542 | from the general TP, we confirm the general monsoon weakening in the KO-S,
543 | observing a substantial Prec decrease of 15% (-11.1 mm y^{-1} , -222 mm), but that is not
544 | significant for all stations. At PYRAMID, the annual loss is relatively comparable with
545 | that of the KO-S (-13.7 mm y^{-1} , -273 mm), but at these high elevations, as we observed
546 | in Table 2, the weather is much more drier (449 and 1527 mm, respectively). Therefore,
547 | the fractional loss is more than 3 times (-52%) that of the KO-S. Considering that the
548 | decreasing trend observed during the summer is more robust than the annual one (see
549 | above), the fractional loss of Prec during the monsoon is -47%, which means that
550 | currently, on average, the precipitation at PYRAMID is the half of what it was twenty
551 | years ago.

552 | At regional level, Turner and Annamalai (2012), using the all-India rainfall data
553 based on a weighted mean of 306 stations, observed a negative precipitation trend since
554 the 1950s in South Asia. According to Yao et al. (2012), using the Global Precipitation
555 Climatology Project (GPCP) data, there is strong evidence that precipitation from 1979
556 to 2010 decreased even in the Himalayas. In eastern CH-S, where the Koshi Basin is
557 located, they estimated a loss of 173 mm, showing a real decreasing trend starting from
558 the early 1990s (mean value between grid 9 and 11 in Fig. S18 of their paper).

559 On the TP, the observed pattern of change is opposite that of the monsoon weakening
560 described by the authors cited above. Liu et al. (2010) described an increase in
561 precipitation in CH-N for the period of the 1980s to 2008. Su et al. (2006) described a
562 marked precipitation increase in the Yangtze River Basin (eastern CH-N). In a similar
563 way to the T analysis, Yang et al. (2006) considered 5 stations located on the northern
564 side of Mt. Everest (therefore, including the two stations also considered in this study)
565 from 1971 to 2004 and observed an increasing, but not significant Prec trend. The
566 higher stationarity we observed is confirmed since 1971 for the two KO-N stations
567 considered in this study.

568 | ~~Different from the north side of Mt. Everest and from the general TP, we confirm the~~
569 ~~general monsoon weakening in the KO-S, observing a substantial Prec decrease of 15%~~
570 ~~(-11.1 mm a⁻¹, 222 mm), but that is not significant for all stations. At PYRAMID, the~~
571 ~~annual loss is relatively comparable with that of the KO-S (13.7 mm a⁻¹, 273 mm), but~~
572 ~~at these high elevations, as we observed in Table 2, the weather is much more drier (449~~
573 ~~and 1527 mm, respectively). Therefore, the fractional loss is more than 3 times (52%)~~
574 ~~that of the KO-S. Considering that the decreasing trend observed during the summer is~~
575 ~~more robust than the annual one (see above), the fractional loss of Prec during the~~
576 ~~monsoon is 47%, which means that currently, on average, the precipitation at~~
577 ~~PYRAMID is the half of what it was twenty years ago.~~

578 6.4 Mechanisms responsible for temperature warming and precipitation weakening

579 According to Rangwala and Miller (2012), there are a number of mechanisms that
580 can cause enhanced warming rates at high elevation, and they often have strong
581 seasonal dependency. These mechanisms arise from either elevation based differential
582 changes in climate drivers, such as snow cover, clouds, specific humidity, aerosols, and
583 soil moisture, or differential sensitivities of surface warming to changes in these drivers
584 at different elevations. This study does not aim to either realize a comprehensive review
585 or to demonstrate the causes that could have led to the climate change pattern observed
586 at PYRAMID, but our intent here is just to note the recent hypotheses advanced in the
587 literature that fit with our observations for the region of investigation.

588 Snow/ice albedo is one of the strongest feedbacks in the climate system (Rangwala
589 and Miller, 2012). Increases in minT are possible if decreases in snow cover are
590 accompanied by increases in soil moisture and surface humidity, which can facilitate a
591 greater diurnal retention of the daytime solar energy in the land surface and amplify the

592 longwave heating of the land surface at night (Rangwala et al., 2012). For the Tibetan
593 Plateau, Rikiishi and Nakasato (2006) found that the length of the snow cover season
594 declined at all elevations between 1966 and 2001. Moreover, minT can be enhanced by
595 nighttime increases in cloud cover. However, assessing changes in clouds and
596 quantifying cloud feedbacks will remain challenging in the near term. For the Tibetan
597 Plateau, Duan and Wu (2006) found that low level nocturnal cloud cover increased over
598 the TP between 1961 and 2003 and that these increases explain part of the observed
599 increases in minT.

600 The maxT increase observed here during April ($p < 0.05$ in 2011, Fig. 4b) fits with
601 the warming reported by Pal and Al-Tabbaa (2010) which observed that within the pre-
602 monsoon season only April shows significant changes in maxT in all Indian regions and
603 WH (1901-2003 period). According to Ramanathan et al. (2007), Gautam et al. (2010)
604 argued that the observed warming during the pre-monsoon period (April-June) can be
605 ascribed not only to the global greenhouse warming, but also to the solar radiation ab-
606 sorption caused by the large amount of aerosol (mineral dust mixed with other carbona-
607 ceous material) transported over the Gangetic-Himalayan region. As recently reported
608 by Marinoni et al. (2013), April represents the month for which the transport of absorb-
609 ing carbonaceous aerosol (i.e. black carbon) is maximized in our region of investigation
610 (Khumbu Valley). At this regards Putero et al. (2013) show evidences for a possible in-
611 fluence of open fire occurrence in South Asia particular abundant during this period of
612 the year. However the significant decreasing of maxT observed in May ($p < 0.05$) and
613 the slight significant decreasing during the monsoon months from June to August ($p <$
614 0.10) appear to deviate from the scenario proposed for April. In this respect it should be
615 kept in mind that the radioactive dynamical interactions of aerosol with the monsoon
616 cycle are extremely complex and different processes can interact with each other. As an
617 instance, as reported by Qian et al. (2011), the deposition of absorbing aerosol on snow
618 and the snow albedo feedback processes can play a prominent role in Himalayas and TP
619 inducing large radioactive flux changes and surface temperature perturbation.

620 Recent studies associate the precipitation decrease over India during the second half
621 of 20th century (e.g., Ramanathan et al., 2005; Lau and Kim, 2006) to the significant
622 tropospheric warming over the tropical area from the Indian Ocean to the western
623 Pacific (e.g., Wu, 2005), while westerlies are strengthening (Zhao et al., 2012). Other
624 authors (e.g., Bollasina et al., 2011) attribute the monsoon weakening to human-
625 influenced aerosol emissions. In fact an increase of aerosols over South Asia has been
626 well documented (Ramanathan et al., 2005; Lau and Kim, 2006) and climate model
627 experiments suggest that sulfate aerosol may significantly reduce monsoon precipitation
628 (Mitchell and Johns, 1997). Despite a historical weakening of the monsoon circulation,
629 most studies project an increase of the seasonal monsoon rainfall under global warming.
630 At this regards Levy II et al., 2013 find that the dramatic emission reductions (35%–
631 80%) in anthropogenic aerosols and their precursors projected by Representative
632 Concentration Pathway (RCP) 4.5 (Moss et al., 2010) result an increasing trend by the
633 second half of the 21st century in South Asia and in particular over the Himalaya

634 (Palazzi et al., 2013).

635 6.5 Linking climate change patterns observed at high elevation with glacier responses

636 6.5.1 Impact of temperature increase

637 Air temperature and precipitation are the two factors most commonly related to
638 glacier fluctuations. However, there still exists a seasonal gap in order to explain the
639 shrinking of summer accumulation-type glaciers (typical of CH) due to large
640 temperature increases observed in the region during winter (Ueno and Aryal, 2008), as
641 is the case for the south slopes of Mt. Everest. Furthermore, in this study we noted a
642 slightly significant decline in summer maxT and stationary meanT. The real increase of
643 T has been observed for minT, but given the mean elevation of glaciers (5695 m a.s.l. in
644 1992) and the mean elevation range of glacier fronts (4568-4817 m a.s.l. in 1992, mean
645 4817 m a.s.l., 249 m of standard deviation –sd-) (Thakuri et al., 2014), this increase for
646 minT can be most likely considered ineffective for melting processes, since T is still less
647 than 0 °C. This inference can be ascertained analyzing Figure 8, created in order to link
648 temperature increases and altitudinal glacier distribution (data from Thakuri et al.,
649 2014). The 0 °C isotherms, corresponding to the mean monthly minT and maxT, are
650 plotted for 1994 and 2013. The elevation of each 0 °C isotherm is calculated according
651 to the accurate lapse rates computation carried out in this study and the observed
652 monthly T trends. We can note that in 1994 the 0 °C isotherm for minT reached the
653 elevation band characterizing the glacier fronts only from June to September. However,
654 | twenty years later, the upward of the 0 °C isotherm is modest (± 92 m) during these
655 months, compared to the huge but ineffective rise for melting processes (downstream
656 | from the glacier fronts) of December-November (even ± 854 m). The maxT has
657 obviously a greater potential impact on glaciers. In fact the 0 °C isotherm for of all
658 months except January and February crosses the elevation bands within which the
659 glacier fronts are located ever since 1994. In this regard we observe that only April
660 | (± 224 m), December (± 212 m), and November (± 160 m) experienced an upward of the
661 0 °C isotherm able to enhance the melting processes, but only close to the glaciers
662 fronts. We therefore point out that the impact caused by the increased temperature
663 occurring in April most likely plays an important role not only in relation to this case
664 study, but also at the level of the Himalayan range. In fact, as mentioned above, Pal and
665 Al-Tabbaa (2010), observed that within the pre-monsoon season, only April showed
666 significant changes in maxT in all Indian regions and WH (1901-2003 period).

667 6.5.2 Impact of precipitation decrease

668

669 As regards the precipitation, in this study we noted a strong and significant
670 decreasing Prec trend for all months, corresponding to a fractional loss of 47% during
671 the monsoon season which indicates that, on average, the precipitation at PYRAMID is
672 currently half of what it was twenty years ago. This climate change pattern confirms and

673 clarifies the observation of Thakuri et al. (2014), who noted that the southern Mt.
674 Everest glaciers experienced a shrinkage acceleration over the last twenty years (1992-
675 2011), as underlined by an upward shift of SLA with a velocity almost three times
676 greater than the previous period (1962-1992). The authors, without the support of
677 climatic data, proposed the hypothesis that Mt. Everest glaciers are shrinking faster
678 since the early 1990s mainly as a result of a weakening of precipitation over the last
679 decades. In fact they observed a double upward shift in the SLA of the largest glaciers
680 (south-oriented and with a higher altitude accumulation zone): a clear signal of a
681 significant decrease in accumulation. Wagnon et al. (2013) have recently reached the
682 same conclusion, but also in this case without the support of any climatic studies. Bolch
683 et al. (2011) and Nuimura et al. (2012) registered a higher mass loss rate during the last
684 decade (2000–2010).

685 Furthermore Quincey et al. (2009) and Peters et al. (2010) observed lower glacier
686 flow velocity in the region over the last decades. Many studies highlight how the
687 present condition of ice stagnation of glaciers in the Mt Everest region, and in general
688 in CH-S, is attributable to low flow velocity generated by generally negative mass
689 balances (Bolch et al., 2008; Quincey et al., 2009; Scherler et al., 2011). Our
690 observations allow attributing the lower glacier flow velocity to lower accumulation due
691 to weaker precipitation, which can thus be considered the main climatic factor driving
692 the current ice stagnation of tongues. In this regard we need to keep in mind that
693 changes in velocity are among the main triggers for the formation of supraglacial and
694 proglacial lakes (Salerno et al., 2012; Quincey et al., 2009), which we know to be
695 susceptible to GLOFs.

696 6.5.3 Trend analysis of annual probability of snowfall

697 Figure 9 analyses how the changes observed for the meanT at PYRAMID have
698 affected the probability of snowfall on total cumulated annual precipitation in the last
699 twenty years. The increase of meanT observed outside the monsoon period, when the
700 precipitation is almost completely composed by snow (Fig. 2), brought a significant
701 decrease of solid phase ($+0.7\% \text{ a}^+ \text{y}^{-1}$, $p < 0.05$). Extending this analysis to the elevation
702 bands characterizing the glaciers distribution (see Fig. 8), through the temperature lapse
703 rate calculated here, we observe that at the level of the mean glaciers (5695 m a.s.l.) the
704 probability of snowfall is stationary ($+0.04\% \text{ a}^+ \text{y}^{-1}$), while it decreases at the mean
705 elevation of SLAs (5345 m a.s.l. in 1992, Thakuri et al., 2014), but not significantly ($-$
706 $0.38\% \text{ a}^+ \text{y}^{-1}$, $p > 0.1$). The reduction becomes significant at lower altitudes. In
707 particular, at the mean elevation of glacier fronts (4817 m a.s.l.) the probability of
708 snowfall is $-0.56\% \text{ a}^+ \text{y}^{-1}$ ($p < 0.05$), i.e. at these altitudes the probability of snow on
709 annual base is currently 11 % ($p < 0.05$) less than twenty years ago. We can conclude
710 this analysis summarizing that a significant change in precipitation phase has occurred
711 close to the terminal portions of glaciers, corresponding broadly to the glaciers ablation
712 zones (around 10 %, $p < 0.5$), while the lower temperature of the upper glaciers zones

713 has so far guaranteed a stationary condition.

714 **Conclusion**

715 Most relevant studies on temperature trends were conducted on the Tibetan Plateau,
716 the Indian subcontinent (including the WH) and the Upper Indus Basin, while studies
717 on the mountainous regions along the southern slope of the central Himalayas in Nepal
718 (CH-S) are limited. Although Shrestha et al. (1999) analyzed the maximum temperature
719 trends over Nepal during the period 1971–1994, studies on recent temperature trends
720 over CH-S are still lacking and, before this study, completely absent as regards high
721 elevation. This paper addresses seasonal variability of minimum, maximum, and mean
722 temperatures and precipitation at high elevation on the southern slopes of Mt. Everest.
723 Moreover, we complete this analysis with data from all the existing weather stations
724 located on both sides of the Himalayan range (Koshi Basin) for the 1994-2013 period,
725 during which a rapider glacier mass loss occurred.

726 At high elevation on the southern slopes of Mt. Everest, we observed the following:

- 727 1) The main increases in air temperature are almost completely concentrated during
728 the post-monsoon months. The pre-monsoon period experienced a slighter and
729 insignificant increase, while the monsoon season is generally stationary. This
730 seasonal temperature change pattern is shared with the entire Koshi Basin, and it
731 is also observed in the regional studies related to the northern and southern
732 slopes of the Himalayan range. Surprisingly, ~~at high elevation~~above 5000 m
733 a.s.l. the maximum temperature decreases significantly in May and slightly
734 during the monsoon months from June to August.
- 735 2) The minimum temperature increased much more than the maximum
736 temperature. This remarkable minimum temperature trend is more similar to the
737 pattern of change commonly described on the Tibetan Plateau and confirmed in
738 this study in the northern Koshi Basin. However, this trend is in contrast with
739 studies located south of the Himalayan ridge. As proved by this study, the
740 southern Koshi Basin experienced a prevalence of maximum temperature
741 increases. No linear pattern emerges in the elevation dependency of temperature
742 trends. We only observed higher minimum temperature trends at higher
743 altitudes.
- 744 3) The total annual precipitation has considerably decreased. The annual rate of
745 decrease ~~at high elevation~~above 5000 m a.s.l. is similar to the one ~~at~~ lower
746 altitudes on the southern side of the Koshi Basin, but the drier conditions of this
747 remote environment make the fractional loss relatively more consistent. The
748 precipitation at high elevation during the monsoon period is currently half of
749 what it was twenty years ago. These observations confirm the monsoon
750 weakening observed by previous studies in India and even in the Himalayas
751 since the early 1980s. As opposed to the northern side of the Koshi Basin that
752 shows in this study certain stability, as positive or stationary trends have been

753 observed by previous studies on the TP and more specifically in northern central
754 Himalaya.

755 4) There is a significantly lower probability of snowfall in the glaciers ablation
756 zones, while the lower temperature of the upper glaciers zones have so far
757 guaranteed a stationary condition.

758 In general, this study contributes to change the perspective on how the climatic
759 driver (temperature vs. precipitation) led the glacier responses in the last twenty years.
760 ~~to a change perspective related to the climatic driver (temperature vs. precipitation) led~~
761 ~~the glacier responses in the last twenty years.~~

762 Without demonstrating the causes that could have led to the climate change pattern
763 observed at the PYRAMID, we simply note the recent literature on hypotheses that
764 accord with our observations. ~~for the case study.~~

765 In conclusion, we have here observed that weather stations at low elevations are not
766 able to suitably describe the climate changes occurring ~~at high altitudes~~ above 5000 m
767 a.s.l. and thus correctly interpret the impact observed on the cryosphere. This
768 consideration stresses the great importance of long-term ground measurements at high
769 elevation.

770 **Author contributions**

771 G.T., Y.M. and E.V. designed research; F.S. performed research; F.S., N.G., S.T., G.V.
772 and E.R. analyzed data; F.S., N.G., E.R. and G.T. wrote the paper. P.C., P.S., N.G. and
773 G.A. data quality check.

774 **Acknowledgements**

775 This work was supported by the MIUR through Ev-K2-CNR/SHARE and CNR-
776 DTA/NEXTDATA project within the framework of the Ev-K2-CNR and Nepal
777 Academy of Science and Technology (NAST). Sudeep Thakuri is recipient of the IPCC
778 Scholarship Award under the collaboration between the IPCC Scholarship Programme
779 and the Prince Albert II of Monaco Foundation's Young Researchers Scholarships
780 Initiative.

781 **References**

782 [Abebe, A., Solomatine, D., and Venneker, R.: Application of adaptive fuzzy rule based](#)
783 [models for reconstruction of missing precipitation events, Hydrolog. Sci. J., 45, 425–](#)
784 [436, doi:10.1080/02626660009492339, 2000.](#)

785 [Abudu, S., Bawazir, A. S., and King, J. P.: Infilling missing daily evapotranspiration](#)
786 [data using neural networks, J. Irrig. Drain. E-asce, 136, 317–325,](#)
787 [doi:10.1061/\(ASCE\)IR.1943-4774.0000197, 2010.](#)

788 [Amatya, L. K., Cuccillato, E., Haack, B., Shadie, P., Sattar, N., Bajracharya, B.,](#)
789 [Shrestha, B. Caroli, P., Panzeri, D., Basani, M., Schommer, B., Flury, B. Salerno, F.,](#)

790 [and Manfredi, E. C.: Improving communication for management of social-ecological](#)
791 [systems in high mountain areas: Development of methodologies and tools – The](#)
792 [HKKH Partnership Project, Mt. Res. Dev., 30, 69-79, doi:10.1659/MRD-JOURNAL-](#)
793 [D-09-00084.1, 2010.](#)

794 [Bajracharya B., Uddin, K., Chettri, N., Shrestha, B., and Siddiqui, S. A.: Understanding](#)
795 [land cover change using a harmonized classification system in the Himalayas: A case](#)
796 [study from Sagarmatha National Park, Nepal, Mt. Res. Dev., 30, 143–156, doi:](#)
797 [10.1659/MRD-JOURNAL-D-09-00044.1, 2010.](#)

798 [Barros, A. P., Kim, G., Williams, E., and Nesbitt, S. W.: Probing orographic controls in](#)
799 [the Himalayas during the monsoon using satellite imagery, Nat. Hazards Earth Syst.](#)
800 [Sci. 4, 29–51, doi:10.5194/nhess-4-29-2004, 2004.](#)

801 [Benn, D. I., Bolch, T., Hands, K., Gulley, J., Luckman, A., Nicholson, L. I., Quincey,](#)
802 [D., Thompson, S., Toumi, R., and Wiseman, S.: Response of debris-covered glaciers](#)
803 [in the Mount Everest region to recent warming, and implications for outburst flood](#)
804 [hazards, Earth-Sci. Rev., 114, 156–174, doi:10.1016/j.earscirev.2012.03.008, 2012.](#)

805 [Bertolani L., Bollasina, M., and Tartari, G.: Recent biannual variability of](#)
806 [meteorological features in the Eastern Highland Himalayas, Geophys. Res. Lett., 27,](#)
807 [2185-2188, doi:10.1029/1999GL011198, 2000.](#)

808 [Bhutiyan, M. R., Kale, V. S., and Pawar, N. J.: Long-term trends in maximum,](#)
809 [minimum and mean annual air temperatures across the Northwestern Himalaya](#)
810 [during the twentieth century, Climatic Change, 85, 159–177, doi:10.1007/s10584-](#)
811 [006-9196-1, 2007.](#)

812 [Bocchiola, D. and Diolaiuti, G.: Evidence of climate change within the Adamello](#)
813 [Glacier of Italy, Theor. Appl. Climatol., 100, 351–369, doi:10.1007/s00704-009-](#)
814 [0186-x, 2010.](#)

815 [Bolch T., Buchroithner, M., Pieczonka, T., and Kunert, A.: Planimetric and volumetric](#)
816 [glacier changes in the Khumbu Himal, Nepal, since 1962 using Corona, Landsat TM](#)
817 [and ASTER data, J. Glaciol., 54, 592–600, doi: 0.3189/002214308786570782, 2008.](#)

818 [Bolch T., Kulkarni, A., Käab, A., Huggel, C., Paul, F., Cogley, J. G., Frey, H., Kargel, J.](#)
819 [S., Fujita, K., Scheel, M., Bajracharya, S., and Stoffel, M.: The state and fate of](#)
820 [Himalayan glaciers, Science, 336, 310-314, doi: 10.1126/science.1215828, 2012.](#)

821 [Bolch T., Pieczonka, T., and Benn, D.I.: Multi-decadal mass loss of glaciers in the](#)
822 [Everest area \(Nepal Himalaya\) derived from stereo imagery, The Cryosphere, 5,](#)
823 [349–358, doi:10.5194/tc-5-349-2011, 2011.](#)

824 [Bollasina, M. A., Ming, Y., and Ramaswamy, V.: Anthropogenic aerosols and the](#)
825 [weakening of the south Asian summer monsoon, Science, 334, 502-505,](#)
826 [doi:10.1126/science.1204994, 2011.](#)

827 [Bookhagen, B. and Burbank, D. W.: Topography, relief, and TRMM-derived rainfall](#)
828 [variations along the Himalaya, Geophys. Res. Lett., 33, L08405,](#)
829 [doi:10.1029/2006GL026037, 2006.](#)

830 [Carraro, E., Guyennon, N., Hamilton, D., Valsecchi, L., Manfredi, E. C., Viviano, G.,](#)
831 [Salerno, F., Tartari, G., and Copetti, D.: Coupling high-resolution measurements to a](#)

832 [three-dimensional lake model to assess the spatial and temporal dynamics of the](#)
833 [cyanobacterium *Planktothrix rubescens* in a medium-sized lake, *Hydrobiologia*, 698](#)
834 [\(1\), 77-95. doi:10.1007/s10750-012-1096-y, 2012.](#)

835 [Carraro, E., Guyennon, N., Viviano, G., Manfredi, E. C., Valsecchi, L., Salerno, F.,](#)
836 [Tartari, G., and Copetti, D.: Impact of Global and Local Pressures on the Ecology of](#)
837 [a Medium-Sized Pre-Alpine Lake, in *Models of the Ecological Hierarchy*, edited by:](#)
838 [Jordan, F., and Jorgensen, S. E., Elsevier B.V., pp. 259-274, doi:10.1016/B978-0-](#)
839 [444-59396-2.00016-X, 2012b.](#)

840 [Coulibaly, P. and Evora, N.: Comparison of neural network methods for infilling](#)
841 [missing daily weather records, *J. Hydrol.*, 341, 27–41,](#)
842 [doi:10.1016/j.jhydrol.2007.04.020, 2007.](#)

843 [Déqué, M.: Frequency of precipitation and temperature extremes over France in an](#)
844 [anthropogenic scenario: model results and statistical correction according to](#)
845 [observed values, *Global Planet. Change*, 57, 16–26,](#)
846 [doi:10.1016/j.gloplacha.2006.11.030, 2007.](#)

847 [Duan, A. and Wu, G.: Change of cloud amount and the climate warming on the Tibetan](#)
848 [Plateau, *Geophys. Res. Lett.*, 33, L22704, doi:10.1029/2006GL027946, 2006.](#)

849 [Dytham, C.: *Choosing and Using Statistics: A Biologist's Guide*, John Wiley & Sons,](#)
850 [2011.](#)

851 [Fujita, K., and Sakai, A.: Modelling runoff from a Himalayan debris-covered glacier,](#)
852 [Hydrol. Earth Syst. Sci., 18, 2679–2694, doi:10.5194/hess-18-2679-2014, 2014.](#)

853 [Fujita, K., Sakai, A., Takenaka, S., Nuimura, T., Surazakov, A. B., Sawagaki, T., and](#)
854 [Yamanokuchi T.: Potential flood volume of Himalayan glacial lakes, *Nat. Hazards*](#)
855 [Earth Syst. Sci., 13, 1827–1839, doi:10.5194/nhessd-1-15-2013, 2013.](#)

856 [Ganguly, N. D. and Iyer, K. N.: Long-term variations of surface air temperature during](#)
857 [summer in India, *Int. J. Climatol.*, 29, 735–746, doi:10.1002/joc.1748, 2009.](#)

858 [Gardelle, J., Arnaud, Y., and Berthier, E.: Contrasted evolution of glacial lakes along the](#)
859 [Hindu Kush Himalaya mountain range between 1990 and 2009, *Global Planet.*](#)
860 [Change, 75, 47-55, doi:10.1016/j.gloplacha.2010.10.003, 2011.](#)

861 [Gautam, R., Hsu, N. C. and Lau, K. M.: Premonsoon aerosol characterization and](#)
862 [radiative effects over the Indo-Gangetic plains: implications for regional climate](#)
863 [warming, *J. Geophys. Res.*, 115, D17208, doi:10.1029/2010JD013819, 2010.](#)

864 [Gerstengarbe, F. W. and Werner, P. C.: Estimation of the beginning and end of recurrent](#)
865 [events within a climate regime, *Clim. Res.*, 11, 97-107, 1999.](#)

866 [Guyennon, N., Romano, E., Portoghese, I., Salerno, F., Calmanti, S., Petrangeli, A. B.,](#)
867 [Tartari, G., and Copetti, D.: Benefits from using combined dynamical-statistical](#)
868 [downscaling approaches – lessons from a case study in the Mediterranean region,](#)
869 [Hydrol. Earth Syst. Sc., 17, 705–720, doi:10.5194/hess-17-705-2013, 2013.](#)

870 [Hock, R.: Glacier melt: a review of processes and their modeling, *Prog. Phys. Geog.*,](#)
871 [29, 362-391, doi:10.1191/0309133305pp453ra, 2005.](#)

872 [Ichiyanagi, K., Yamanaka, M. D., Muraji, Y., and Vaidya, B. K.: Precipitation in Nepal](#)
873 [between 1987 and 1996, *Int. J. Climatol.*, 27, 1753–1762, doi:10.1002/joc.1492,](#)

874 [2007.](#)

875 [Immerzeel, W. W., Petersen, L., Ragettli, S., and Pellicciotti, F.: The importance of](#)

876 [observed gradients of air temperature and precipitation for modeling runoff from a](#)

877 [glacierized watershed in the Nepal Himalayas, *Water Resour. Res.*, 50,](#)

878 [doi:10.1002/2013WR014506, 2014.](#)

879 [James, A. L. and Oldenburg, C. M.: Linear and Monte Carlo uncertainty analysis for](#)

880 [subsurface contaminant transport simulation, *Water Resour. Res.*, 33, 2495–2508,](#)

881 [doi:10.1029/97WR01925, 1997.](#)

882 [Kattel, D. B. and Yao, T.: Recent temperature trends at mountain stations on the](#)

883 [southern slope of the central Himalayas, *J. Earth Syst. Sci.*, 122, 215–227, doi:](#)

884 [10.1007/s12040-012-0257-8, 2013.](#)

885 [Kendall, M.G.: Rank Correlation Methods, Oxford University Press, New York, 1975.](#)

886 [Kivekas, N., Sun, J., Zhan, M., Kerminen, V. M., Hyvarinen, A., Komppula, M.,](#)

887 [Viisanen, Y., Hong, N., Zhang, Y., Kulmala, M., Zhang, X. C., Deli-Geer, and](#)

888 [Lihavainen, H.: Long term particle size distribution measurements at Mount](#)

889 [Waliguan, a high-altitude site in inland China, *Atmos. Chem. Phys.*, 9, 5461–5474,](#)

890 [doi:10.5194/acp-9-95461-2009, 2009.](#)

891 [Lami, A., Marchetto, A., Musazzi, S., Salerno, F., Tartari, G., Guilizzoni, P., Rogora, M.,](#)

892 [and Tartari, G. A.: Chemical and biological response of two small lakes in the](#)

893 [Khumbu Valley, Himalayas \(Nepal\) to short-term variability and climatic change as](#)

894 [detected by long-term monitoring and paleolimnological methods, *Hydrobiologia*,](#)

895 [648, 189–205, doi:10.1007/s10750-010-0262-3, 2010.](#)

896 [Lau, K.-M., and Kim, K.-M.: Observational relationships between aerosol and Asian](#)

897 [monsoon rainfall, and circulation, *Geophys. Res. Lett.*, 33, L21810,](#)

898 [doi: 10.1029/2006GL027546, 2006.](#)

899 [Lavagnini, I., Badocco, D., Pastore, P., and Magno, F.: Theil-Sen nonparametric regres-](#)

900 [sion technique on univariate calibration, inverse regression and detection limits, *Ta-*](#)

901 [lanta](#), 87, 180–188, doi:10.1016/j.talanta.2011.09.059, 2011.

902 [Levy II, H., L. W., Horowitz, M. D., Schwarzkopf, Y., Ming, J. C., Golaz, V., Naik, and](#)

903 [Ramaswamy, V.: The roles of aerosol direct and indirect effects in past and future](#)

904 [climate change, *J. Geophys. Res.*, 118, 1–12, doi:10.1002/jgrd.50192, 2013.](#)

905 [Liu, J., Yang, B., and Qin, C.: Tree-ring based annual precipitation reconstruction since](#)

906 [AD 1480 in south central Tibet. *Quatern. Int.*, 236, 75–81,](#)

907 [doi:10.1016/j.quaint.2010.03.020, 2010.](#)

908 [Liu, K., Cheng, Z., Yan, L., and Yin, Z.: Elevation dependency of recent and future min-](#)

909 [imum surface air temperature trends in the Tibetan Plateau and its surroundings,](#)

910 [Global Planet. Change, 68, 164–174, doi:10.1016/j.gloplacha.2009.03.017, 2009.](#)

911 [Liu, X. D., and Chen, B. D.: Climatic warming in the Tibetan Plateau during recent](#)

912 [decades, *Int. J. Climatol.*, 20, 1729–1742, doi:10.1002/1097-](#)

913 [0088\(20001130\)20:14<1729::AID-JOC556>3.0.CO;2-Y, 2000.](#)

914 [Liu, X.D., Yin, Z. Y., Shao, X., and Qin, N.: Temporal trends and variability of daily](#)

915 [maximum and minimum, extreme temperature events, and growing season length](#)

916 [over the eastern and central Tibetan Plateau during 1961–2003, *J. Geophys. Res.*,](#)
917 [111, D19, doi:10.1029/2005JD006915, 2006.](#)

918 [Manfredi, E. C., Flury, B., Viviano, G., Thakuri, S., Khanal, S. N., Jha, P. K., Maskey,](#)
919 [R. K., Kayastha, R. B., Kafle, K. R., Bhochhibhoya, S., Ghimire, N. P., Shrestha, B.](#)
920 [B., Chaudhary, G., Giannino, F., Carteni, F., Mazzoleni, S., and Salerno, F.: Solid](#)
921 [waste and water quality management models for Sagarmatha National Park and](#)
922 [Buffer Zone, Nepal: implementation of a participatory modeling framework, *Mt.*](#)
923 [Res. Dev.](#), 30, 127-142, doi:10.1659/MRD-JOURNAL-D-10-00028.1, 2010.

924 [Marinoni, A., Cristofanelli, P., Laj, P., Putero, D., Calzolari, F., Landi, T. C., Vuillermoz,](#)
925 [E., Maione, M., and Bonasoni, P.: High black carbon and ozone concentrations](#)
926 [during pollution transport in the Himalayas: Five years of continuous observations at](#)
927 [NCO-Prec global GAW station, *J. Environ. Sci.*, 25, 1618–1625, doi:10.1016/S1001-](#)
928 [0742\(12\)60242-3, 2013.](#)

929 [Menne, M. J., Durre, I., Vose, R. S., Gleason, B. E., and Houston, T. G.: An overview of](#)
930 [the Global Historical Climatology Network—daily database, *J. Atmos. Oceanic*](#)
931 [Technol.](#), 29, 897–910, 2012.

932 [Mitchell, J. F. B. and Johns, T. C.: On the modification of global warming by sulphate](#)
933 [aerosols. *J. Climate*, 10, 245-267, 1997.](#)

934 [Montgomery, D. R. and Stolar, D. B.: Reconsidering Himalayan river anticlines,](#)
935 [Geomorphology](#), 82, 4–15, doi:10.1016/j.geomorph.2005.08.021, 2006.

936 [Moss, R. H., et al.: The next generation of scenarios for climate change research and](#)
937 [assessment, *Nature*, 463, 747–756, doi:10.1038/nature08823, 2010.](#)

938 [Nuimura, T., Fujita, K., Yamaguchi, S., and Sharma, R. R.: Elevation changes of](#)
939 [glaciers revealed by multitemporal digital elevation models calibrated by GPS survey](#)
940 [in the Khumbu region, Nepal Himalaya, 1992–2008, *J. Glaciol.*, 58, 648–656, doi:](#)
941 [10.3189/2012JoG11J061, 2012.](#)

942 [Pal, I. and Al-Tabbaa, A.: Long-term changes and variability of monthly extreme tem-](#)
943 [peratures in India, *Theor. Appl. Climatol.*, 100, 45–56, doi:10.1007/s00704-009-](#)
944 [0167-0, 2010.](#)

945 [Palazzi, E., von Hardenberg, J., and Provenzale, A.: Precipitation in the Hindu-Kush](#)
946 [Karakoram Himalaya: Observations and future scenarios, *J. Geophys. Res.*, 118, 85-](#)
947 [100, doi: 10.1029/2012JD018697, 2013.](#)

948 [Pepin, N. C. and Lundquist, J. D.: Temperature trends at high elevations: patterns across](#)
949 [the globe, *Geophys. Res. Lett.*, 35, doi:10.1029/2008GL034026, 2008.](#)

950 [Peters, J., Bolch, T., Buchroithner, M. F., and Bäbler, M.: Glacier Surface Velocities in](#)
951 [the Mount Everest Area/Nepal using ASTER and Ikonos imagery, Proceeding of 10th](#)
952 [International Symposium on High Mountain Remote Sensing Cartography,](#)
953 [Kathmandu, Nepal, 313-320, 2010.](#)

954 [Putero, D., T. C., Landi, P., Cristofanelli, A., Marinoni, P., Laj, R., Duchi, F., Calzolari,](#)
955 [G. P., Verza and P. Bonasoni, Influence of open vegetation fires on black carbon and](#)
956 [ozone variability in the southern Himalayas \(NCO-P, 5079 m a.s.l.\), *Environ. Pollut.*,](#)
957 [184, 597-604, doi: 10.1016/j.envpol.2013.09.035, 2013.](#)

958 [Qian, Y., Flanner, M., Leung, L., and Wang, W.: Sensitivity studies on the impacts of](#)
959 [Tibetan plateau snowpack pollution on the Asian hydrological cycle and monsoon](#)
960 [climate, Atmos. Chem. Phys., 11, 1929–1948, doi:10.5194/acp-11-1929-2011, 2011.](#)
961 [Quincey, D. J., Luckman, A., and Benn, D.: Quantification of Everest region glacier ve-](#)
962 [locities between 1992 and 2002, using satellite radar interferometry and feature](#)
963 [tracking, J. Glaciol., 55, 596-606, doi: 10.3189/002214309789470987, 2009.](#)
964 [Ramanathan, V., Chung, C., Kim, D., Bettge, T., Buja, L., Kiehl, J. T., Washington, W.](#)
965 [M., Fu, Q., Sikka, D. R., and Wild, M.: Atmospheric brown clouds: Impacts on South](#)
966 [Asian climate and hydrological cycle. Proc. Natl. Acad. Sci. U.S.A., 102, 5326- 5333,](#)
967 [doi: 10.1073/pnas.0500656102, 2005.](#)
968 [Ramanathan, V., Li, F., Ramana, M. V., Praveen, P. S., Kim, D., Corrigan, C. E.,](#)
969 [Nguyen, H., Stone, E. A., Schauer, J. J., Carmichael, G. R., Adhikary, B., and Yoon,](#)
970 [S. C.: Atmospheric brown clouds: Hemispherical and regional variations in long-](#)
971 [range transport, absorption, and radiative forcing, J. Geophys. Res., 112, D22,](#)
972 [doi:10.1029/2006JD008124, 2007.](#)
973 [Rangwala, I. and Miller, J. R.: Climate change in mountains: a review of elevation-](#)
974 [dependent warming and its possible causes, Climatic Change, 114, 527–547,](#)
975 [doi:10.1007/s10584-012-0419-3, 2012.](#)
976 [Rangwala, I., Barsugli, J., Cozzetto, K., Neff, J., and Prairie, J.: Mid-21st century](#)
977 [projections in temperature extremes in the southern Colorado Rocky Mountains from](#)
978 [regional climate models, Clim Dyn., 39, 1823-1840, doi:10.1007/s00382- 011-1282-](#)
979 [z, 2012.](#)
980 [Rikiishi, K. and Nakasato, H.: Height dependence of the tendency for reduction in](#)
981 [seasonal snow cover in the Himalaya and the Tibetan Plateau region, 1966–2001,](#)
982 [Ann. Glaciol., 43, 369–377, doi: http://dx.doi.org/10.3189/172756406781811989,](#)
983 [2006.](#)
984 [Salerno, F., Buraschi, E., Bruccoleri, G., Tartari, G., and Smiraglia, C.: Glacier surface-](#)
985 [area changes in Sagarmatha National Park, Nepal, in the second half of the 20th cen-](#)
986 [tury, by comparison of historical maps, J. Glaciol., 54, 738-752, 2008.](#)
987 [Salerno, F., Cuccillato, E., Caroli, P., Bajracharya, B., Manfredi, E. C., Viviano, G.,](#)
988 [Thakuri, S., Flury, B., Basani, M., Giannino, F., and Panzeri, D.: Experience with a](#)
989 [hard and soft participatory modeling framework for social ecological system man-](#)
990 [agement in Mount Everest \(Nepal\) and K2 \(Pakistan\) protected areas, Mt. Res. Dev.,](#)
991 [30, 80-93, 2010a.](#)
992 [Salerno, F., Gambelli, S., Viviano, G., Thakuri, S., Guyennon, N., D’Agata, C.,](#)
993 [Diolaiuti, G., Smiraglia, C., Stefani, F., Bochiola, D., and Tartari, G.: High alpine](#)
994 [ponds shift upwards as average temperature increase: A case study of the Ortles-](#)
995 [Cevedale mountain group \(Southern alps, Italy\) over the last 50 years, Global Planet.](#)
996 [Change, doi: 10.1016/j.gloplacha.2014.06.003, 2014.](#)
997 [Salerno, F., Thakuri, S., D’Agata, C., Smiraglia, C., Manfredi, E. C., Viviano, G., and](#)
998 [Tartari, G.: Glacial lake distribution in the Mount Everest region: Uncertainty of](#)
999 [measurement and conditions of formation, Global Planet. Change, 92-93, 30-39,](#)

1000 [doi:10.1016/j.gloplacha.2012.04.001](https://doi.org/10.1016/j.gloplacha.2012.04.001), 2012.

1001 [Salerno, F., Viviano, G., Mangredi, E. C., Caroli, P., Thakuri, S., and Tartari, G.: Multiple Carrying Capacities from a management-oriented perspective to operationalize sustainable tourism in protected area, J. Environ. Manage., 128, 116-125, doi:10.1016/j.jenvman.2013.04.043, 2013.](#)

1002

1003

1004

1005 [Salerno, F., Viviano, G., Thakuri, S., Flury, B., Maskey, R. K., Khanal, S. N., Bhujju, D., Carrer, M., Bhochhibhoya, S., Melis, M. T., Giannino, F., Staiano, A., Carteni, F., Mazzoleni, S., Cogo, A., Sapkota, A., Shrestha, S., Pandey, R. K., and Manfredi, E. C.: Energy, forest, and indoor air pollution models for Sagarmatha National Park and Buffer zone, Nepal: implementation of a participatory modeling framework, Mt. Res. Dev., 30, 113–126, 2010b.](#)

1006

1007

1008

1009

1010

1011 [Scherler, D., Bookhagen, B., and Strecker, M. R.: Spatially variable response of Himalayan glaciers to climate change affected by debris cover. Nature Geosci., 4, 156–159, doi:10.1038/ngeo1068, 2011.](#)

1012

1013

1014 [Schneider, T.: Analysis of incomplete climate data: Estimation of mean values and covariance matrices and imputation of missing values, J. Clim., 14, 853–871, doi:10.1175/1520-0442\(2001\)014<0853:AOICDE>2.0.CO;2, 2001.](#)

1015

1016

1017 [Sellegri, K., Laj, P., Venzac, H., Boulon, J., Picard, D., Villani, P., Bonasoni, P., Marinoni, A., Cristofanelli, P., and Vuillermoz, E.: Seasonal variations of aerosol size distributions based on long-term measurements at the high altitude Himalayan site of Nepal Climate Observatory—Pyramid \(5079 m\), Nepal, Atmos. Chem. Phys., 10, 10679–10690, doi:10.5194/acp-10.10679-2010, 2010.](#)

1018

1019

1020

1021

1022 [Sen, P. K.: Estimates of the regression coefficient based on Kendall’s Tau, J. Am. Assoc., 63, 1379-1389, doi:10.2307/2285891, 1968.](#)

1023

1024 [Shekhar, M. S., Chand, H., Kumar, S., Srinivasan, K., and Ganju, A.: Climate-change studies in the western Himalaya, Ann. Glaciol., 51, 105-112, doi:10.3189/172756410791386508, 2010.](#)

1025

1026

1027 [Shrestha, A. B., Wake, C. P., Mayewski, P. A., and Dibb, J. E.: Maximum temperature trends in the Himalaya and its vicinity: An analysis based on temperature records from Nepal for the period 1971-94, J. Clim., 12, 2775-5561, doi:10.1175/1520-0442\(1999\)012<2775:MTTITH>2.0.CO;2, 1999.](#)

1028

1029

1030

1031 [Singh, P. and Kumar, N.: Effect of orography on precipitation in the western Himalayan region, J. Hydrol., 199, 183-206, doi:10.1016/S0022-1694\(96\)03222-2, 1997.](#)

1032

1033 [Su, B. D., Jiang, T., and Jin, W. B.: Recent trends in observed temperature and precipitation extremes in the Yangtze River basin, China, Theor. Appl. Climatol., 83, 139–151, doi:10.1007/s00704-005-0139-y, 2006.](#)

1034

1035

1036 [Tartari, G., Salerno, F., Buraschi, E., Bruccoleri, G., and Smiraglia, C.: Lake surface area variations in the North-Eastern sector of Sagarmatha National Park \(Nepal\) at the end of the 20th Century by comparison of historical maps, J. Limnol., 67, 139-154, doi:10.4081/jlimnol.2008.139, 2008.](#)

1037

1038

1039

1040 [Tartari, G., Verza, P., and Bertolami, L.: Meteorological data at PYRAMID Observatory Laboratory \(Khumbu Valley, Sagarmatha National Park, Nepal\), in Limnology of](#)

1041

1042 [high altitude lakes in the Mt. Everest Region \(Nepal\), edited by: Lami, A. and](#)
1043 [Giussani, G., Mem. Ist. Ital. Idrobiol, 57, 23-40, 2002.](#)

1044 [Tartari, G., Vuillermoz, E., Manfredi, E. C., and Toffolon, R.: CEOP High Elevations](#)
1045 [Initiative, GEWEX News, Special Issue, 19\(3\), 4-5, 2009.](#)

1046 [Thakuri, S., Salerno, F., Smiraglia, C., Bolch, T., D'Agata, C., Viviano, G., and Tartari,](#)
1047 [G.: Tracing glacier changes since the 1960s on the south slope of Mt. Everest \(central](#)
1048 [southern Himalaya\) using optical satellite imagery, The Cryosphere, 8, 1297-1315,](#)
1049 [doi:10.5194/tc-8-1297-2014, 2014.](#)

1050 [Themeßl, M. J., Gobiet, A., and Heinrich, G.: Empirical-statistical downscaling and](#)
1051 [error correction of regional climate models and its impact on the climate change](#)
1052 [signal, Climatic Change, 112, 449-468, doi:10.1007/s10584-011-011-0224-4, 2012.](#)

1053 [Turner, A. G. and Annamalai, H.: Climate change and the South Asian summer](#)
1054 [monsoon, Nat. Clim. Change, 2, 587-595, doi:10.1038/nclimate1495, 2012.](#)

1055 [Ueno K. and Aryal, R.: Impact of tropical convective activity on monthly temperature](#)
1056 [variability during non monsoon season in the Nepal Himalayas, J. Geophys. Res.,](#)
1057 [113, D18112, doi:10.1029/2007JD009524, 2008.](#)

1058 [Ueno, K., Endoh, N., Ohata, T., Yabuki, H., Koike, M., and Zhang, Y.: Characteristics of](#)
1059 [precipitation distribution in Tangula, Monsoon, 1993, Bulletin of Glaciological](#)
1060 [Research, 12, 39-46, 1994.](#)

1061 [UNEP \(United Nations Environment Programme\)/WCMC \(World Conservation](#)
1062 [Monitoring Centre\): Sagarmatha National Park, Nepal, in Encyclopedia of Earth,](#)
1063 [edited by: McGinley, M. and Cleveland, C. J., Environmental Information Coalition,](#)
1064 [National Council for Science and the Environment, Washington, DC, 2008.](#)

1065 [Venzac, H., Sellegri, K., Laj, P., Villani, P., Bonasoni, P., Marinoni, A., Cristofanelli, P.,](#)
1066 [Calzolari, F., Fuzzi, S., Decesari, S., Facchini, M. C., Vuillermoz, E., and Verza, G. P.:](#)
1067 [High frequency new particle formation in the Himalayas, Proc. Natl. Acad. Sci.](#)
1068 [USA, 105, 15666-15671, doi:10.1073/pnas.0801355105, 2008.](#)

1069 [Vuille, M.: Climate variability and high altitude temperature and precipitation, in](#)
1070 [Encyclopedia of snow, ice and glaciers, edited by: Singh, V. P. et al., Springer, pp.](#)
1071 [153-156, 2011.](#)

1072 [Wagnon, P., Vincent, C., Arnaud, Y., Berthier, E., Vuillermoz, E., Gruber, S., Ménégoz,](#)
1073 [M., Gilbert, A., Dumont, M., Shea, J. M., Stumm, D., and Pokhrel, B. P.: Seasonal](#)
1074 [and annual mass balances of Mera and Pokalde glaciers \(Nepal Himalaya\) since](#)
1075 [2007, The Cryosphere, 7, 1769-1786, doi:10.5194/tc-7-1769-2013, 2013.](#)

1076 [Washington, W. M. and Parkinson, C. L.: An introduction to three-Dimensional Climate](#)
1077 [Modeling, 2nd Edition, University Science Books, Sausalito, 2005.](#)

1078 [Wu, B.: Weakening of Indian summer monsoon in recent decades, Adv. Atmos. Sci.](#)
1079 [22\(1\), 21-29, doi:10.1007/BF02930866, 2005.](#)

1080 [Yang J., Tan, C., and Zhang, T.: Spatial and temporal variations in air temperature and](#)
1081 [precipitation in the Chinese Himalayas during the 1971–2007, Int. J. Climatol., 33,](#)
1082 [2622-2632, doi:10.1002/joc.3609, 2012.](#)

1083 [Yang, X., Zhang, Y., Zhang, W., Yan, Y., Wang, Z., Ding, M., and Chu, D.: Climate](#)

1084 [change in Mt. Qomolangma region since 1971, *J. Geogr. Sci.*, 16, 326-336,](#)
1085 [doi:10.1007/s11442-006-0308-7, 2006.](#)

1086 [Yao, T., Thompson, L., Yang, W., Yu, W., Gao, Y., Guo, X., Yang, X., Duan, K., Zhao,](#)
1087 [H., Xu, B., Pu, J., Lu, A., Xiang, Y., Kattel, D. B., and Joswiak, D.: Different glacier](#)
1088 [status with atmospheric circulations in Tibetan Plateau and surroundings, *Nat. Clim.*](#)
1089 [Change, 2, 663-667, doi:10.1038/nclimate1580, 2012.](#)

1090 [Yasutomi, N., Hamada, A., and Yatagai, A.: Development of a long-term daily gridded](#)
1091 [temperature dataset and its application to rain/snow discrimination of daily](#)
1092 [precipitation, *Global Environ. Res.*, V15N2, 165-172, 2011.](#)

1093 [You, Q., Kang, S., Pepin, N., Flügel, W., Yan, Y., Behrawan, H., and Huang, J.: Rela-](#)
1094 [tionship between temperature trend magnitude, elevation and mean temperature in](#)
1095 [the Tibetan Plateau from homogenized surface stations and reanalysis data, *Global*](#)
1096 [Planet. Change, 71, 124-133, doi:10.1016/j.gloplacha.2010.01.020, 2010.](#)

1097 [Zhao, H., Xu, B., Yao, T., Wu, G., Lin, S., Gao, J., and Wang, M.: Deuterium excess](#)
1098 [record in a southern Tibetan ice core and its potential climatic implications, *Clim.*](#)
1099 [Dyn., 38, 1791-1803, doi:10.1007/s00382-011-1161-7, 2012.](#)

1100

1101 ~~Fujita, K., and Sakai, A.: Modelling runoff from a Himalayan debris-covered glacier,~~
1102 ~~Hydrol. Earth Syst. Sci., 18, 2679–2694, doi:10.5194/hess-18-2679-2014, 2014.~~

1103 ~~Ueno, K., Endoh, N., Ohata, T., Yabuki, H., Koike, M., and Zhang, Y.: Characteristics of~~
1104 ~~precipitation distribution in Tangula, Monsoon, 1993, Bulletin of Glaciological~~
1105 ~~Research, 12, 39–46, 1994.~~

1106 ~~Abebe, A., Solomatine, D., and Venneker, R.: Application of adaptive fuzzy rule based~~
1107 ~~models for reconstruction of missing precipitation events, Hydrolog. Sci. J., 45, 425–~~
1108 ~~436, doi:10.1080/02626660009492339, 2000.~~

1109 ~~Abudu, S., Bawazir, A. S., and King, J. P.: Infilling missing daily evapotranspiration~~
1110 ~~data using neural networks, J. Irrig. Drain. E-asc, 136, 317–325,~~
1111 ~~doi:10.1061/(ASCE)IR.1943-4774.0000197, 2010.~~

1112 ~~Amatya, L. K., Cuccillato, E., Haack, B., Shadie, P., Sattar, N., Bajracharya, B.,~~
1113 ~~Shrestha, B., Caroli, P., Panzeri, D., Basani, M., Schommer, B., Flury, B., Salerno, F.,~~
1114 ~~and Manfredi, E. C.: Improving communication for management of social-ecological~~
1115 ~~systems in high mountain areas: Development of methodologies and tools—The~~
1116 ~~HKKH Partnership Project, Mt. Res. Dev., 30, 69–79, doi:10.1659/MRD-JOURNAL-~~
1117 ~~D-09-00084.1, 2010.~~

1118 ~~Bajracharya B., Uddin, K., Chettri, N., Shrestha, B., and Siddiqui, S. A.: Understanding~~
1119 ~~land cover change using a harmonized classification system in the Himalayas: A case~~
1120 ~~study from Sagarmatha National Park, Nepal, Mt. Res. Dev., 30, 143–156, doi:~~
1121 ~~10.1659/MRD-JOURNAL-D-09-00044.1, 2010.~~

1122 ~~Barros, A. P., Kim, G., Williams, E., and Nesbitt, S. W.: Probing orographic controls in~~
1123 ~~the Himalayas during the monsoon using satellite imagery, Nat. Hazards Earth Syst.~~
1124 ~~Sci. 4, 29–51, doi:10.5194/nhess-4-29-2004, 2004.~~

1125 ~~Benn, D. I., Bolch, T., Hands, K., Gulley, J., Luckman, A., Nicholson, L. I., Quincey,~~

1126 D., Thompson, S., Toumi, R., and Wiseman, S.: Response of debris-covered glaciers
1127 in the Mount Everest region to recent warming, and implications for outburst flood
1128 hazards, *Earth Sci. Rev.*, 114, 156–174, doi:10.1016/j.earseirev.2012.03.008, 2012.

1129 Bertolani L., Bollasina, M., and Tartari, G.: Recent biannual variability of
1130 meteorological features in the Eastern Highland Himalayas, *Geophys. Res. Lett.*, 27,
1131 2185–2188, doi:10.1029/1999GL011198, 2000.

1132 Bhutiyani, M. R., Kale, V. S., and Pawar, N. J.: Long-term trends in maximum,
1133 minimum and mean annual air temperatures across the Northwestern Himalaya
1134 during the twentieth century, *Climatic Change*, 85, 159–177, doi:10.1007/s10584-
1135 006-9196-1, 2007.

1136 Bocchiola, D. and Diolaiuti, G.: Evidence of climate change within the Adamello
1137 Glacier of Italy, *Theor. Appl. Climatol.*, 100, 351–369, doi:10.1007/s00704-009-
1138 0186-x, 2010.

1139 Bolch T., Kulkarni, A., Käab, A., Huggel, C., Paul, F., Cogley, J. G., Frey, H., Kargel, J.
1140 S., Fujita, K., Scheel, M., Bajracharya, S., and Stoffel, M.: The state and fate of
1141 Himalayan glaciers, *Science*, 336, 310–314, doi: 10.1126/science.1215828, 2012.

1142 Bolch T., Buchroithner, M., Pieczonka, T., and Kunert, A.: Planimetric and volumetric
1143 glacier changes in the Khumbu Himal, Nepal, since 1962 using Corona, Landsat TM
1144 and ASTER data, *J. Glaciol.*, 54, 592–600, doi: 0.3189/002214308786570782, 2008.

1145 Bolch T., Pieczonka, T., and Benn, D.I.: Multi-decadal mass loss of glaciers in the
1146 Everest area (Nepal Himalaya) derived from stereo imagery, *The Cryosphere*, 5,
1147 349–358, doi:10.5194/te-5-349-2011, 2011.

1148 Bollasina, M. A., Ming, Y., and Ramaswamy, V.: Anthropogenic aerosols and the
1149 weakening of the south Asian summer monsoon, *Science*, 334, 502–505,
1150 doi:10.1126/science.1204994, 2011.

1151 Bookhagen, B. and Burbank, D. W.: Topography, relief, and TRMM-derived rainfall
1152 variations along the Himalaya, *Geophys. Res. Lett.*, 33, L08405,
1153 doi:10.1029/2006GL026037, 2006.

1154 Carraro, E., Guyennon, N., Hamilton, D., Valsecchi, L., Manfredi, E. C., Viviano, G.,
1155 Salerno, F., Tartari, G., and Copetti, D.: Coupling high-resolution measurements to a
1156 three-dimensional lake model to assess the spatial and temporal dynamics of the
1157 cyanobacterium *Planktothrix rubescens* in a medium-sized lake, *Hydrobiologia*, 698
1158 (1), 77–95. doi:10.1007/s10750-012-1096-y, 2012.

1159 Carraro, E., Guyennon, N., Viviano, G., Manfredi, E. C., Valsecchi, L., Salerno, F.,
1160 Tartari, G., and Copetti, D.: Impact of Global and Local Pressures on the Ecology of
1161 a Medium-Sized Pre-Alpine Lake, in *Models of the Ecological Hierarchy*, edited by:
1162 Jordan, F., and Jorgensen, S. E., Elsevier B.V., pp. 259–274, doi:10.1016/B978-0-
1163 444-59396-2.00016-X, 2012b.

1164 Coulibaly, P. and Evora, N.: Comparison of neural network methods for infilling
1165 missing daily weather records, *J. Hydrol.*, 341, 27–41,
1166 doi:10.1016/j.jhydrol.2007.04.020, 2007.

1167 Déqué, M.: Frequency of precipitation and temperature extremes over France in an

1168 anthropogenic scenario: model results and statistical correction according to
1169 observed values, *Global Planet. Change*, 57, 16–26,
1170 doi:10.1016/j.gloplacha.2006.11.030, 2007.

1171 Duan, A. and Wu, G.: Change of cloud amount and the climate warming on the Tibetan
1172 Plateau, *Geophys. Res. Lett.*, 33, L22704, doi:10.1029/2006GL027946, 2006.

1173 Dytham, C.: *Choosing and Using Statistics: A Biologist's Guide*, John Wiley & Sons,
1174 2011.

1175 Fujita, K., Sakai, A., Takenaka, S., Nuimura, T., Surazakov, A. B., Sawagaki, T., and
1176 Yamanokuchi T.: Potential flood volume of Himalayan glacial lakes, *Nat. Hazards*
1177 *Earth Syst. Sci.*, 13, 1827–1839, doi:10.5194/nhessd-1-15-2013, 2013.

1178 Ganguly, N. D. and Iyer, K. N.: Long term variations of surface air temperature during
1179 summer in India, *Int. J. Climatol.*, 29, 735–746, doi:10.1002/joc.1748, 2009.

1180 Gardelle, J., Arnaud, Y., and Berthier, E.: Contrasted evolution of glacial lakes along the
1181 Hindu Kush Himalaya mountain range between 1990 and 2009, *Global Planet.*
1182 *Change*, 75, 47–55, doi:10.1016/j.gloplacha.2010.10.003, 2011.

1183 Gautam, R., Hsu, N. C. and Lau, K. M.: Premonsoon aerosol characterization and
1184 radiative effects over the Indo Gangetic plains: implications for regional climate
1185 warming, *J. Geophys. Res.*, 115, D17208, doi:10.1029/2010JD013819, 2010.

1186 Gerstengarbe, F. W. and Werner, P. C.: Estimation of the beginning and end of recurrent
1187 events within a climate regime, *Clim. Res.*, 11, 97–107, 1999.

1188 Guyennon, N., Romano, E., Portoghesi, I., Salerno, F., Calmanti, S., Petrangeli, A. B.,
1189 Tartari, G., and Copetti, D.: Benefits from using combined dynamical statistical
1190 downscaling approaches—lessons from a case study in the Mediterranean region,
1191 *Hydrol. Earth Syst. Sc.*, 17, 705–720, doi:10.5194/hess-17-705-2013, 2013.

1192 Hoek, R.: Glacier melt: a review of processes and their modeling, *Prog. Phys. Geog.*,
1193 29, 362–391, doi:10.1191/0309133305pp453ra, 2005.

1194 Ichiyonagi, K., Yamanaka, M. D., Muraji, Y., and Vaidya, B. K.: Precipitation in Nepal
1195 between 1987 and 1996, *Int. J. Climatol.*, 27, 1753–1762, doi:10.1002/joc.1492,
1196 2007.

1197 Immerzeel, W. W., Petersen, L., Raetelli, S., and Pellicciotti, F.: The importance of
1198 observed gradients of air temperature and precipitation for modeling runoff from a
1199 glacierized watershed in the Nepal Himalayas, *Water Resour. Res.*, 50,
1200 doi:10.1002/2013WR014506, 2014.

1201 James, A. L. and Oldenburg, C. M.: Linear and Monte Carlo uncertainty analysis for
1202 subsurface contaminant transport simulation, *Water Resour. Res.*, 33, 2495–2508,
1203 doi:10.1029/97WR01925, 1997.

1204 Kattel, D. B. and Yao, T.: Recent temperature trends at mountain stations on the
1205 southern slope of the central Himalayas, *J. Earth Syst. Sci.*, 122, 215–227, doi:
1206 10.1007/s12040-012-0257-8, 2013.

1207 Kendall, M.G.: *Rank Correlation Methods*, Oxford University Press, New York, 1975.

1208 Kivekas, N., Sun, J., Zhan, M., Kerminen, V. M., Hyvarinen, A., Komppula, M.,
1209 Viisanen, Y., Hong, N., Zhang, Y., Kulmala, M., Zhang, X. C., Deli-Geer, and

1210 ~~Lihavainen, H.: Long term particle size distribution measurements at Mount~~
1211 ~~Waliguan, a high altitude site in inland China, *Atmos. Chem. Phys.*, 9, 5461–5474,~~
1212 ~~doi:10.5194/acp-9-95461-2009, 2009.~~

1213 ~~Lami, A., Marchetto, A., Musazzi, S., Salerno, F., Tartari, G., Guilizzoni, P., Rogora, M.,~~
1214 ~~and Tartari, G. A.: Chemical and biological response of two small lakes in the~~
1215 ~~Khumbu Valley, Himalayas (Nepal) to short term variability and climatic change as~~
1216 ~~detected by long term monitoring and paleolimnological methods, *Hydrobiologia*,~~
1217 ~~648, 189–205, doi:10.1007/s10750-010-0262-3, 2010.~~

1218 ~~Lau, K. M., and Kim, K. M.: Observational relationships between aerosol and Asian~~
1219 ~~monsoon rainfall, and circulation, *Geophys. Res. Lett.*, 33, L21810,~~
1220 ~~doi: 10.1029/2006GL027546, 2006.~~

1221 ~~Lavagnini, I., Badoeco, D., Pastore, P., and Magno, F.: Theil-Sen nonparametric regres-~~
1222 ~~sion technique on univariate calibration, inverse regression and detection limits, *Ta-*~~
1223 ~~lanta~~, 87, 180–188, doi:10.1016/j.talanta.2011.09.059, 2011.

1224 ~~Levy H, H., L. W., Horowitz, M. D., Schwarzkopf, Y., Ming, J. C., Golaz, V., Naik, and~~
1225 ~~Ramaswamy, V.: The roles of aerosol direct and indirect effects in past and future~~
1226 ~~climate change, *J. Geophys. Res.*, 118, 1–12, doi:10.1002/jgrd.50192, 2013.~~

1227 ~~Liu, J., Yang, B., and Qin, C.: Tree-ring based annual precipitation reconstruction since~~
1228 ~~AD 1480 in south central Tibet. *Quatern. Int.*, 236, 75–81,~~
1229 ~~doi:10.1016/j.quaint.2010.03.020, 2010.~~

1230 ~~Liu, K., Cheng, Z., Yan, L., and Yin, Z.: Elevation dependency of recent and future min-~~
1231 ~~imum surface air temperature trends in the Tibetan Plateau and its surroundings,~~
1232 ~~*Global Planet. Change*, 68, 164–174, doi:10.1016/j.gloplacha.2009.03.017, 2009.~~

1233 ~~Liu, X. D., and Chen, B. D.: Climatic warming in the Tibetan Plateau during recent~~
1234 ~~decades, *Int. J. Climatol.*, 20, 1729–1742, doi:10.1002/1097-~~
1235 ~~0088(20001130)20:14<1729::AID-JOC556>3.0.CO;2-Y, 2000.~~

1236 ~~Liu, X.D., Yin, Z. Y., Shao, X., and Qin, N.: Temporal trends and variability of daily~~
1237 ~~maximum and minimum, extreme temperature events, and growing season length~~
1238 ~~over the eastern and central Tibetan Plateau during 1961–2003, *J. Geophys. Res.*,~~
1239 ~~111, D19, doi:10.1029/2005JD006915, 2006.~~

1240 ~~Manfredi, E. C., Flury, B., Viviano, G., Thakuri, S., Khanal, S. N., Jha, P. K., Maskey,~~
1241 ~~R. K., Kayastha, R. B., Kafle, K. R., Bhochhibhoya, S., Ghimire, N. P., Shrestha, B.~~
1242 ~~B., Chaudhary, G., Giannino, F., Carteni, F., Mazzoleni, S., and Salerno, F.: Solid~~
1243 ~~waste and water quality management models for Sagarmatha National Park and~~
1244 ~~Buffer Zone, Nepal: implementation of a participatory modeling framework, *Mt.*~~
1245 ~~*Res. Dev.*, 30, 127–142, doi:10.1659/MRD-JOURNAL-D-10-00028.1, 2010.~~

1246 ~~Marinoni, A., Cristofanelli, P., Laj, P., Putero, D., Calzolari, F., Landi, T. C., Vuillermoz,~~
1247 ~~E., Maione, M., and Bonasoni, P.: High black carbon and ozone concentrations~~
1248 ~~during pollution transport in the Himalayas: Five years of continuous observations at~~
1249 ~~NCO-Prec global GAW station, *J. Environ. Sci.*, 25, 1618–1625, doi:10.1016/S1001-~~
1250 ~~0742(12)60242-3, 2013.~~

1251 ~~Mitchell, J. F. B. and Johns, T. C.: On the modification of global warming by sulphate~~

1252 aerosols. *J. Climate*, 10, 245–267, 1997.

1253 ~~Montgomery, D. R. and Stolar, D. B.: Reconsidering Himalayan river anticlines,~~
1254 ~~Geomorphology~~, 82, 4–15, doi:10.1016/j.geomorph.2005.08.021, 2006.

1255 ~~Moss, R. H., et al.: The next generation of scenarios for climate change research and~~
1256 ~~assessment~~, *Nature*, 463, 747–756, doi:10.1038/nature08823, 2010.

1257 ~~Numura, T., Fujita, K., Yamaguchi, S., and Sharma, R. R.: Elevation changes of~~
1258 ~~glaciers revealed by multitemporal digital elevation models calibrated by GPS survey~~
1259 ~~in the Khumbu region, Nepal Himalaya, 1992–2008~~, *J. Glaciol.*, 58, 648–656, doi:
1260 ~~10.3189/2012JoG11J061~~, 2012.

1261 ~~Pal, I. and Al-Tabbaa, A.: Long term changes and variability of monthly extreme tem-~~
1262 ~~peratures in India~~, *Theor. Appl. Climatol.*, 100, 45–56, doi:10.1007/s00704-009-
1263 ~~0167-0~~, 2010.

1264 ~~Palazzi, E., von Hardenberg, J., and Provenzale, A.: Precipitation in the Hindu Kush~~
1265 ~~Karakoram Himalaya: Observations and future scenarios~~, *J. Geophys. Res.*, 118, 85-
1266 ~~100~~, doi: 10.1029/2012JD018697, 2013.

1267 ~~Pepin, N. C. and Lundquist, J. D.: Temperature trends at high elevations: patterns across~~
1268 ~~the globe~~, *Geophys. Res. Lett.*, 35, doi:10.1029/2008GL034026, 2008.

1269 ~~Peters, J., Boleh, T., Buchroithner, M. F., and Bäßler, M.: Glacier Surface Velocities in~~
1270 ~~the Mount Everest Area/Nepal using ASTER and Ikonos imagery~~, *Proceeding of 10th*
1271 ~~International Symposium on High Mountain Remote Sensing Cartography,~~
1272 ~~Kathmandu, Nepal~~, 313–320, 2010.

1273 ~~Putero, D., T. C., Landi, P., Cristofanelli, A., Marinoni, P., Laj, R., Duchi, F., Calzolari,~~
1274 ~~G. P., Verza and P. Bonasoni, Influence of open vegetation fires on black carbon and~~
1275 ~~ozone variability in the southern Himalayas (NCO-P, 5079 m a.s.l.)~~, *Environ. Pollut.*,
1276 ~~184~~, 597–604, doi: 10.1016/j.envpol.2013.09.035, 2013.

1277 ~~Qian, Y., Flanner, M., Leung, L., and Wang, W.: Sensitivity studies on the impacts of~~
1278 ~~Tibetan plateau snowpack pollution on the Asian hydrological cycle and monsoon~~
1279 ~~climate~~, *Atmos. Chem. Phys.*, 11, 1929–1948, doi:10.5194/acp-11-1929-2011, 2011.

1280 ~~Quincey, D. J., Luckman, A., and Benn, D.: Quantification of Everest region glacier ve-~~
1281 ~~locities between 1992 and 2002, using satellite radar interferometry and feature~~
1282 ~~tracking~~, *J. Glaciol.*, 55, 596–606, doi: 10.3189/002214309789470987, 2009.

1283 ~~Ramanathan, V., Chung, C., Kim, D., Bettge, T., Buja, L., Kiehl, J. T., Washington, W.~~
1284 ~~M., Fu, Q., Sikka, D. R., and Wild, M.: Atmospheric brown clouds: Impacts on South~~
1285 ~~Asian climate and hydrological cycle~~. *Proc. Natl. Acad. Sci. U.S.A.*, 102, 5326–5333,
1286 ~~doi: 10.1073/pnas.0500656102~~, 2005.

1287 ~~Ramanathan, V., Li, F., Ramana, M. V., Praveen, P. S., Kim, D., Corrigan, C. E.,~~
1288 ~~Nguyen, H., Stone, E. A., Schauer, J. J., Carmichael, G. R., Adhikary, B., and Yoon,~~
1289 ~~S. C.: Atmospheric brown clouds: Hemispherical and regional variations in long-~~
1290 ~~range transport, absorption, and radiative forcing~~, *J. Geophys. Res.*, 112, D22,
1291 ~~doi:10.1029/2006JD008124~~, 2007.

1292 ~~Rangwala, I. and Miller, J. R.: Climate change in mountains: a review of elevation-~~
1293 ~~dependent warming and its possible causes~~, *Climatic Change*, 114, 527–547,

1294 ~~doi:10.1007/s10584-012-0419-3, 2012.~~

1295 ~~Rangwala, I., Barsugli, J., Cozzetto, K., Neff, J., and Prairie, J.: Mid 21st century~~

1296 ~~projections in temperature extremes in the southern Colorado Rocky Mountains from~~

1297 ~~regional climate models, *Clim Dyn.*, 39, 1823–1840, doi:10.1007/s00382-011-1282-~~

1298 ~~z, 2012.~~

1299 ~~Rikiishi, K. and Nakasato, H.: Height dependence of the tendency for reduction in~~

1300 ~~seasonal snow cover in the Himalaya and the Tibetan Plateau region, 1966–2001,~~

1301 ~~*Ann. Glaciol.*, 43, 369–377, doi: http://dx.doi.org/10.3189/172756406781811989,~~

1302 ~~2006.~~

1303 ~~Salerno, F., Buraschi, E., Bruccoleri, G., Tartari, G., and Smiraglia, C.: Glacier surface-~~

1304 ~~area changes in Sagarmatha National Park, Nepal, in the second half of the 20th cen-~~

1305 ~~tury, by comparison of historical maps, *J. Glaciol.*, 54, 738–752, 2008.~~

1306 ~~Salerno, F., Viviano, G., Mangredi, E. C., Caroli, P., Thakuri, S., and Tartari, G.: Multi-~~

1307 ~~ple Carrying Capacities from a management oriented perspective to operationalize~~

1308 ~~sustainable tourism in protected area, *J. Environ. Manage.*, 128, 116–125,~~

1309 ~~doi:10.1016/j.jenvman.2013.04.043, 2013.~~

1310 ~~Salerno, F., Gambelli, S., Viviano, G., Thakuri, S., Guyennon, N., D’Agata, C.,~~

1311 ~~Diolaiuti, G., Smiraglia, C., Stefani, F., Boehhiola, D., and Tartari, G.: High alpine~~

1312 ~~ponds shift upwards as average temperature increase: A case study of the Ortles-~~

1313 ~~Cevedale mountain group (Southern alps, Italy) over the last 50 years, *Global Planet.*~~

1314 ~~*Change*, doi: 10.1016/j.gloplacha.2014.06.003, 2014.~~

1315 ~~Salerno, F., Thakuri, S., D’Agata, C., Smiraglia, C., Manfredi, E. C., Viviano, G., and~~

1316 ~~Tartari, G.: Glacial lake distribution in the Mount Everest region: Uncertainty of~~

1317 ~~measurement and conditions of formation, *Global Planet. Change*, 92–93, 30–39,~~

1318 ~~doi:10.1016/j.gloplacha.2012.04.001, 2012.~~

1319 ~~Scherler, D., Bookhagen, B., and Strecker, M.R.: Spatially variable response of Himala-~~

1320 ~~yan glaciers to climate change affected by debris cover. *Nature Geosci.*, 4, 156–159,~~

1321 ~~doi:10.1038/ngeo1068, 2011.~~

1322 ~~Schneider, T.: Analysis of incomplete climate data: Estimation of mean values and~~

1323 ~~covariance matrices and imputation of missing values, *J. Clim.*, 14, 853–871,~~

1324 ~~doi:10.1175/1520-0442(2001)014<0853:AOICDE>2.0.CO;2, 2001.~~

1325 ~~Sellegrì, K., Laj, P., Venzac, H., Boulon, J., Picard, D., Villani, P., Bonasoni, P.,~~

1326 ~~Marinoni, A., Cristofanelli, P., and Vuillermoz, E.: Seasonal variations of aerosol size~~

1327 ~~distributions based on long-term measurements at the high-altitude Himalayan site of~~

1328 ~~Nepal Climate Observatory Pyramid (5079 m), Nepal, *Atmos. Chem. Phys.*, 10,~~

1329 ~~10679–10690, doi:10.5194/acp-10.10679-2010, 2010.~~

1330 ~~Sen, P. K.: Estimates of the regression coefficient based on Kendall’s Tau, *J. Am.*~~

1331 ~~*Assoc.*, 63, 1379–1389, doi:10.2307/2285891, 1968.~~

1332 ~~Shekhar, M. S., Chand, H., Kumar, S., Srinivasan, K., and Ganju, A.: Climate change~~

1333 ~~studies in the western Himalaya, *Ann. Glaciol.*, 51, 105–112,~~

1334 ~~doi:10.3189/172756410791386508, 2010.~~

1335 ~~Shrestha, A. B., Wake, C. P., Mayewski, P. A., and Dibb, J. E.: Maximum temperature~~

1336 trends in the Himalaya and its vicinity: An analysis based on temperature records
1337 from Nepal for the period 1971-94, *J. Clim.*, 12, 2775-5561, doi:10.1175/1520-
1338 0442(1999)012<2775:MTTITH>2.0.CO;2, 1999.

1339 Singh, P. and Kumar, N.: Effect of orography on precipitation in the western Himalayan
1340 region, *J. Hydrol.*, 199, 183-206, doi:10.1016/S0022-1694(96)03222-2, 1997.

1341 Su, B. D., Jiang, T., and Jin, W. B.: Recent trends in observed temperature and
1342 precipitation extremes in the Yangtze River basin, China, *Theor. Appl. Climatol.*, 83,
1343 139-151, doi:10.1007/s00704-005-0139-y, 2006.

1344 Tartari, G., Vuillermoz, E., Manfredi, E. C., and Toffolon, R.: CEOP High Elevations
1345 Initiative, *GEWEX News, Special Issue*, 19(3), 4-5, 2009.

1346 Tartari, G., Salerno, F., Buraschi, E., Bruccoleri, G., and Smiraglia, C.: Lake surface
1347 area variations in the North-Eastern sector of Sagarmatha National Park (Nepal) at
1348 the end of the 20th Century by comparison of historical maps, *J. Limnol.*, 67, 139-
1349 154, doi:10.4081/jlimnol.2008.139, 2008.

1350 Tartari, G., Verza, P., and Bertolami, L.: Meteorological data at PYRAMID Observatory
1351 Laboratory (Khumbu Valley, Sagarmatha National Park, Nepal), in *Limnology of
1352 high altitude lakes in the Mt. Everest Region (Nepal)*, edited by: Lami, A. and
1353 Giussani, G., *Mem. Ist. Ital. Idrobiol.*, 57, 23-40, 2002.

1354 Thakuri, S., Salerno, F., Smiraglia, C., Bolch, T., D'Agata, C., Viviano, G., and Tartari,
1355 G.: Tracing glacier changes since the 1960s on the south slope of Mt. Everest (central
1356 southern Himalaya) using optical satellite imagery, *The Cryosphere*, 8, 1297-1315,
1357 doi:10.5194/te-8-1297-2014, 2014.

1358 Themeßl, M. J., Gobiet, A., and Heinrich, G.: Empirical-statistical downscaling and
1359 error correction of regional climate models and its impact on the climate change
1360 signal, *Climatic Change*, 112, 449-468, doi:10.1007/s10584-011-011-0224-4, 2012.

1361 Turner, A. G. and Annamalai, H.: Climate change and the South Asian summer
1362 monsoon, *Nat. Clim. Change*, 2, 587-595, doi:10.1038/nclimate1495, 2012.

1363 Ueno K. and Aryal, R.: Impact of tropical convective activity on monthly temperature
1364 variability during non-monsoon season in the Nepal Himalayas, *J. Geophys. Res.*,
1365 113, D18112, doi:10.1029/2007JD009524, 2008.

1366 UNEP (United Nations Environment Programme)/WCMC (World Conservation
1367 Monitoring Centre): Sagarmatha National Park, Nepal, in *Encyclopedia of Earth*,
1368 edited by: McGinley, M. and Cleveland, C. J., Environmental Information Coalition,
1369 National Council for Science and the Environment, Washington, DC, 2008.

1370 Venzac, H., Sellegri, K., Laj, P., Villani, P., Bonasoni, P., Marinoni, A., Cristofanelli, P.,
1371 Calzolari, F., Fuzzi, S., Decesari, S., Facchini, M. C., Vuillermoz, E., and Verza, G. P.:
1372 High-frequency new particle formation in the Himalayas, *Proc. Natl. Acad. Sci.
1373 USA*, 105, 15666-15671, doi:10.1073/pnas.0801355105, 2008.

1374 Vuille, M.: Climate variability and high-altitude temperature and precipitation, in
1375 *Encyclopedia of snow, ice and glaciers*, edited by: Singh, V. P. et al., Springer, pp.
1376 153-156, 2011.

1377 Wagnon, P., Vincent, C., Arnaud, Y., Berthier, E., Vuillermoz, E., Gruber, S., Ménégoz,

1378 M., Gilbert, A., Dumont, M., Shea, J. M., Stumm, D., and Pokhrel, B. P.: Seasonal
1379 and annual mass balances of Mera and Pokalde glaciers (Nepal Himalaya) since
1380 2007, *The Cryosphere*, 7, 1769–1786, doi:10.5194/te-7-1769-2013, 2013.

1381 Washington, W. M. and Parkinson, C. L.: An introduction to three-Dimensional Climate
1382 Modeling, 2nd Edition, University Science Books, Sausalito, 2005.

1383 Wu, B.: Weakening of Indian summer monsoon in recent decades, *Adv. Atmos. Sci.*
1384 22(1), 21–29, doi:10.1007/BF02930866, 2005.

1385 Yang J., Tan, C., and Zhang, T.: Spatial and temporal variations in air temperature and
1386 precipitation in the Chinese Himalayas during the 1971–2007, *Int. J. Climatol.*, 33,
1387 2622–2632, doi:10.1002/joc.3609, 2012.

1388 Yang, X., Zhang, Y., Zhang, W., Yan, Y., Wang, Z., Ding, M., and Chu, D.: Climate
1389 change in Mt. Qomolangma region since 1971, *J. Geogr. Sci.*, 16, 326–336,
1390 doi:10.1007/s11442-006-0308-7, 2006.

1391 Yao, T., Thompson, L., Yang, W., Yu, W., Gao, Y., Guo, X., Yang, X., Duan, K., Zhao,
1392 H., Xu, B., Pu, J., Lu, A., Xiang, Y., Kattel, D. B., and Joswiak, D.: Different glacier
1393 status with atmospheric circulations in Tibetan Plateau and surroundings, *Nat. Clim.*
1394 *Change*, 2, 663–667, doi:10.1038/nclimate1580, 2012.

1395 You, Q., Kang, S., Pepin, N., Flügel, W., Yan, Y., Behrawan, H., and Huang, J.: Rela-
1396 tionship between temperature trend magnitude, elevation and mean temperature in
1397 the Tibetan Plateau from homogenized surface stations and reanalysis data, *Global*
1398 *Planet. Change*, 71, 124–133, doi:10.1016/j.gloplacha.2010.01.020, 2010.

1399 Zhao, H., Xu, B., Yao, T., Wu, G., Lin, S., Gao, J., and Wang, M.: Deuterium excess
1400 record in a southern Tibetan ice core and its potential climatic implications, *Clim.*
1401 *Dyn.*, 38, 1791–1803, doi:10.1007/s00382-011-1161-7, 2012.

1402

1403 *Table 1. List of surface stations belonging to PYRAMID Observatory Laboratory*
 1404 *network located along the south slopes of Mt. Everest (upper DK Basin).*

Station ID	Location	Latitude °N	Longitude °E	Elevation m a.s.l.	Sampling Frequency	Data Availability		% of daily missing data	
						From	To	Air Temperature	Precipitation
AWS3	Lukla	27.70	86.72	2660	1 hour	02/11/2004	31/12/2012	23	20
AWSN	Namche	27.80	86.71	3570	1 hour	27/10/2001	31/12/2012	21	27
AWS2	Pheriche	27.90	86.82	4260	1 hour	25/10/2001	31/12/2013	15	22
AWS0	Pyramid	27.96	86.81	5035	2 hours	01/01/1994	31/12/2005	19	16
AWS1	Pyramid	27.96	86.81	5035	1 hour	01/01/2000	31/12/2013	10	21
ABC	Pyramid	27.96	86.82	5079	1 hour	01/03/2006	31/12/2011	5	1
AWS4	Kala Patthar	27.99	86.83	5600	10 minutes	01/01/2009	31/12/2013	28	38
AWS5	South Col	27.96	86.93	7986	10 minutes	01/05/2008	31/10/2011	39	100

1405

1406

1407 Table 2. List of ground weather stations located in the Koshi Basin and descriptive
 1408 statistics of the Sen's slopes for minimum, maximum, and mean air temperatures and
 1409 total precipitation for the 1994-2012 period. The annual mean air temperature, the total
 1410 annual mean precipitation, and the percentage of missing daily values is also reported.
 1411 Level of significance ($^{\circ}$ p -value = 0.1, * p -value = 0.05, ** p -value = 0.01, and *** p -
 1412 value = 0.001).

ID	Station Name	Latitude	Longitude	Elevation	Air Temperature					Precipitation				
					Annual mean	Missing values	MinT trend	MaxT Trend	MeanT trend	Annual total	Missing values	Prec trend		
					$^{\circ}\text{C}$	%	$^{\circ}\text{C a}^{-1}$	$^{\circ}\text{C a}^{-1}$	$^{\circ}\text{C a}^{-1}$	mm	%	mm a^{-1}		
		$^{\circ}\text{N}$	$^{\circ}\text{N}$	m a.s.l.										
KO-S (NEPAL)	1024 DHULIKHEL	27.61	85.55	1552	17.1	2	-0.012	0.041	0.026					
	1036 PANCHKHAL	27.68	85.63	865	21.4	10	0.038	0.051 *	0.038 $^{\circ}$	1191	10	-25.0 *		
	1058 TARKE GHYANG	28.00	85.55	2480						3669	10	-21.9		
	1101 NAGDAHA	27.68	86.10	850						1369	3	-1.4		
	1103 JIRI	27.63	86.23	2003	14.4	1	0.013	0.020	0.014 $^{\circ}$	2484	4	6.6		
	1202 CHAURIKHARK	27.70	86.71	2619						2148	2	1.3		
	1206 OKHALDHUNGA	27.31	86.50	1720	17.6	2	-0.017	0.042	0.000	1786	3	-5.1		
	1210 KURULE GHAT	27.13	86.41	497						1017	2	-23.4 $^{\circ}$		
	1211 KHOTANG BAZAR	27.03	86.83	1295						1324	4	15.9		
	1222 DIKTEL	27.21	86.80	1623						1402	6	10.4		
	1301 NUM	27.55	87.28	1497						4537	6	-54.3 **		
	1303 CHAINPUR (EAST)	27.28	87.33	1329	19.1	0	-0.127 *	0.024	-0.064 $^{\circ}$	1469	0	-1.1		
	1304 PAKHRIBAS	27.05	87.28	1680	16.7	0	-0.005	0.036 *	0.015	1540	4	-3.7		
	1307 DHANKUTA	26.98	87.35	1210	20.0	0	-0.002	0.153 ***	0.071 ***	942	6	-9.2 $^{\circ}$		
	1314 TERHATHUM	27.13	87.55	1633	18.2	10	0.033	0.066 $^{\circ}$	0.049 *	1052	6	-13.1 $^{\circ}$		
	1317 CHEPUWA	27.46	87.25	2590						2531	5	-41.9 *		
	1322 MACHUWAGHAT	26.96	87.16	158						1429	6	-22.9 $^{\circ}$		
	1403 LUNGTHUNG	27.55	87.78	1780						2347	1	2.6		
1405 TAPLEJUNG	27.35	87.66	1732	16.6	1	0.060 *	0.085 **	0.071 **	1966	3	-11.6			
1419 PHIDIM	27.15	87.75	1205	21.2	7	0.047 *	0.082 **	0.067 **	1287	2	-13.6 *			
	MEAN	27.33	87.00	1587	17.9	2	0.003	0.060 $^{\circ}$	0.029 $^{\circ}$	1527	4	-11.1		
	PYRAMID	27.96	86.81	5035	-2.4	0	0.072 ***	0.009	0.044 *	449	0	-13.7 ***		
KO-N (TIBET)	DINGRI	28.63	87.08	4,302	3.5	0	0.037 $^{\circ}$	0.041 $^{\circ}$	0.037 *	309	0	-0.1		
	NYALAM	28.18	85.97	3,811	4.1	0	0.032 $^{\circ}$	0.036 $^{\circ}$	0.036 $^{\circ}$	616	0	-0.2		
	MEAN	28.41	86.53	4,057	3.8	0.1	0.034 $^{\circ}$	0.039 *	0.037 *	463	0	-0.1		

1413

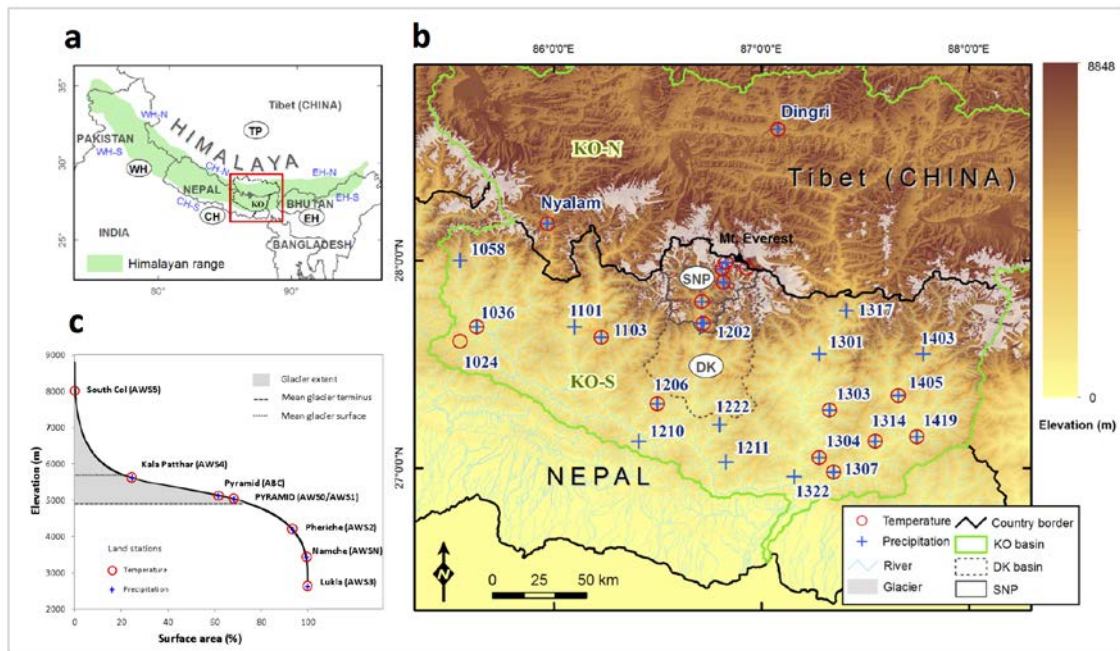
1414

1415 Table 3. Descriptive statistics of the Sen's slopes on a seasonal basis for minimum,
 1416 maximum, and mean air temperatures and total precipitation of weather stations
 1417 located in the Koshi Basin for the 1994-2012 period. The Nepali and Tibetan stations
 1418 are aggregated as mean values. Level of significance ($^{\circ}$ p -value = 0.1, * p -value = 0.05,
 1419 ** p -value = 0.01, and *** p -value = 0.001). Annual and seasonal temperature trends
 1420 are expressed as $^{\circ}\text{C } \alpha^{\pm} \underline{y}^{-1}$. Annual precipitation trend is expressed as $\text{mm } \alpha^{\pm} \underline{y}^{-1}$, while
 1421 the seasonal precipitation trends are in $\text{mm (4 months)} \alpha^{\pm} \underline{y}^{-1}$.

Location	Minimum Temperature				Maximum Temperature				Mean Temperature				Total Precipitation			
	Pre-	Monsoon	Post-	Annual	Pre-	Monsoon	Post-	Annual	Pre-	Monsoon	Post-	Annual	Pre-	Monsoon	Post-	Annual
SOUTHERN KOSHI BASIN (KO-S, NEPAL)	0.012	-0.005	-0.001	0.003	0.076 [*]	0.052	0.069 [*]	0.060 [*]	0.043	0.020	0.030	0.030 [*]	0.8	-8.6	-2.5	-11.1
PYRAMID (NEPAL)	0.067 [*]	0.041 [*]	0.151 ^{***}	0.072 ^{***}	0.024	-0.028	0.049	0.009	0.035	0.015	0.124 ^{**}	0.044 ^{**}	-2.5 ^{**}	-9.3 ^{**}	-1.4 ^{**}	-13.7 ^{***}
NORTHERN KOSHI BASIN (KO-N,TIBET)	0.042 [*]	0.019	0.086 [*]	0.034 [*]	0.023	0.030	0.071 [*]	0.039 [*]	0.042 [*]	0.013	0.084 [*]	0.037 [*]	2.2	0.4	-3.3 [*]	-0.1

1422

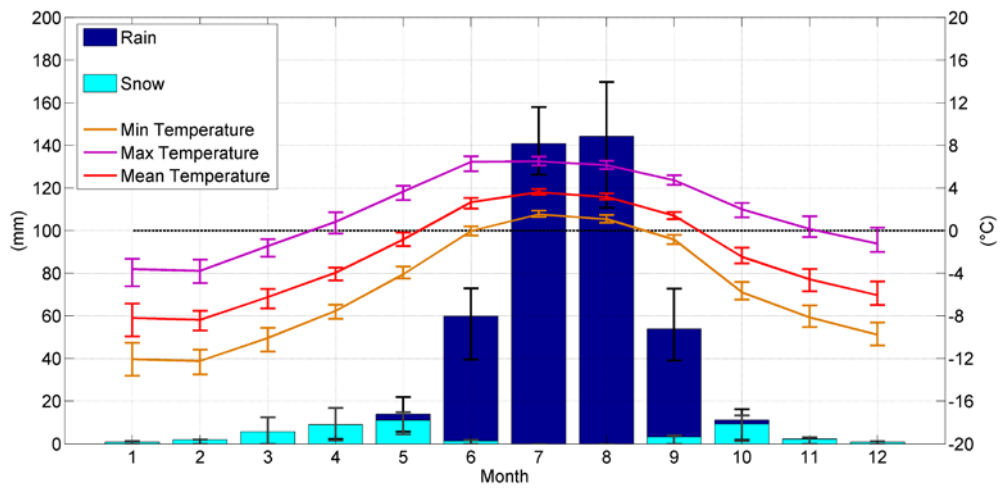
1423



1424

1425 *Figure 1. a) Location of the study area in the Himalaya, where the abbreviations WH,*
 1426 *CH, EH represents the Western, Central and Eastern Himalaya, respectively (the*
 1427 *suffixes -N and -S indicate the northern and southern slopes). b) Focused map on the*
 1428 *spatial distribution of all meteorological stations used in this study, where KO and DK*
 1429 *stand for the Koshi and Dudh Koshi Basins, respectively; SNP represents the*
 1430 *Sagarmatha National Park. c) Hypsometric curve of SNP (upper DK Basin) and*
 1431 *altitudinal glacier distribution. Along this curve, the locations of meteorological*
 1432 *stations belonging to PYRAMID Observatory Laboratory are presented.*

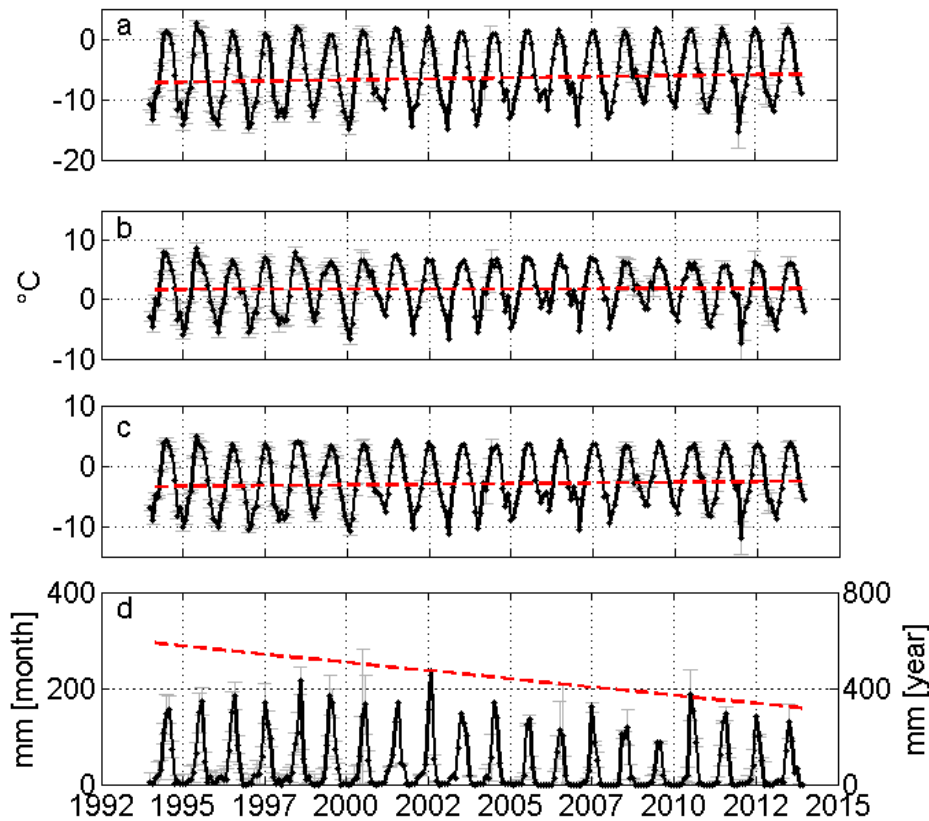
1433



1434

1435 *Figure 2. Mean monthly cumulated precipitation subdivided into snowfall and rainfall*
 1436 *and minimum, maximum, and mean temperature at 5050 m a.s.l. (reference period*
 1437 *1994-2013). The bars represent the standard deviation.*

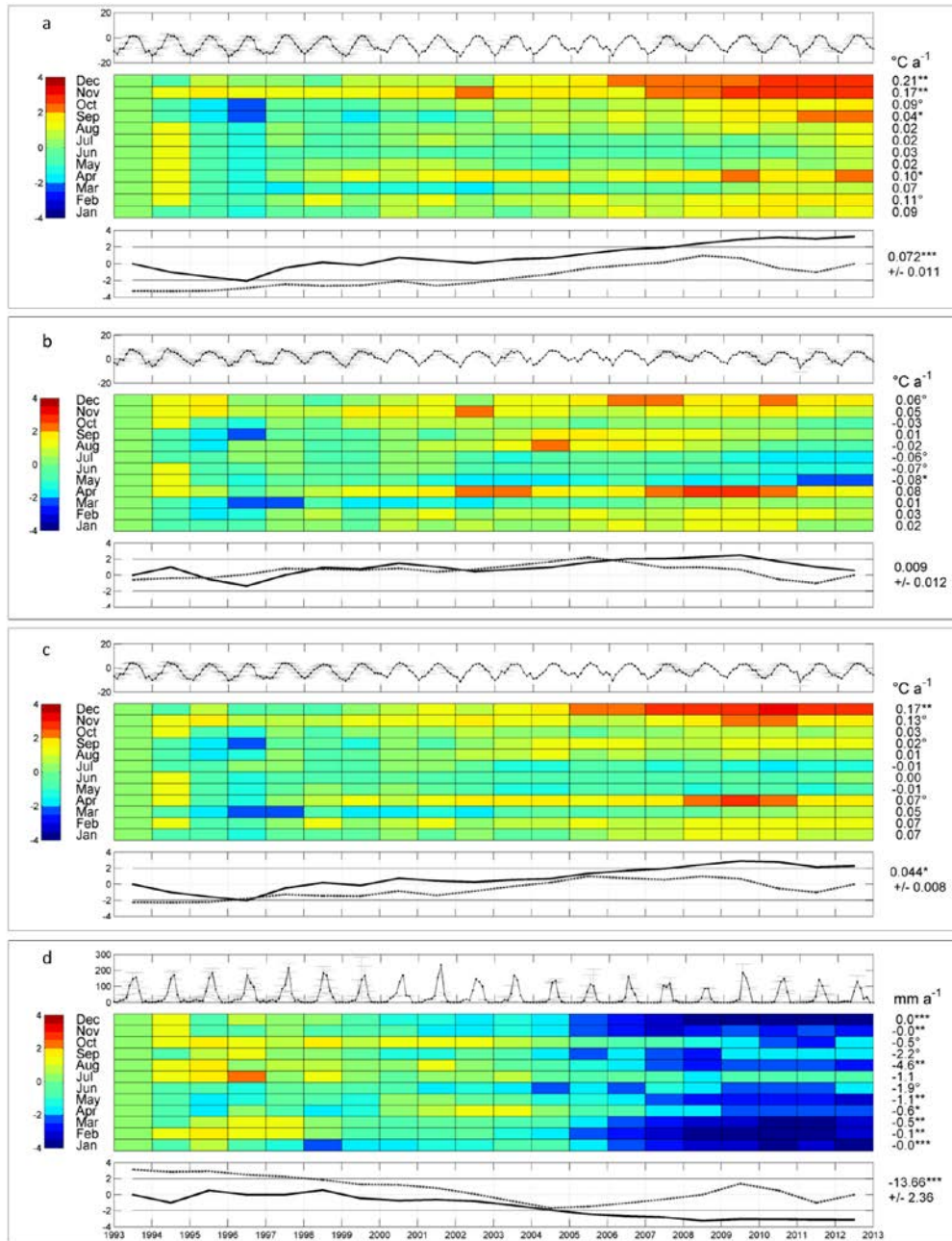
1438



1439

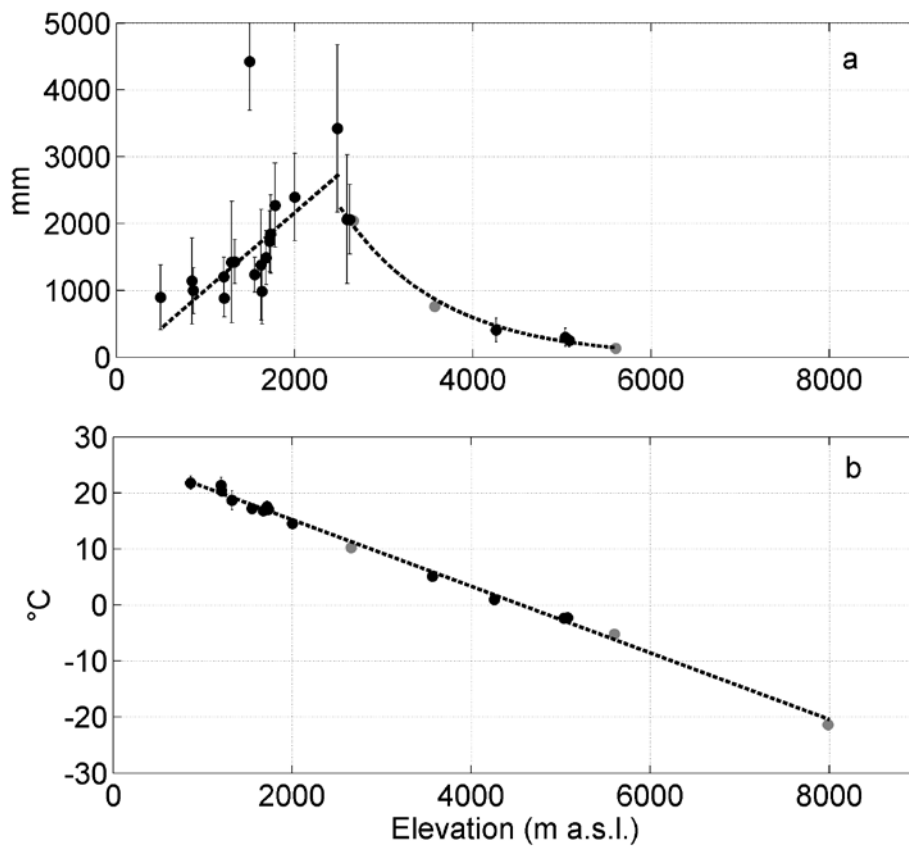
1440 *Figure 3. Temperature and precipitation monthly time series (1994-2013) reconstructed*
 1441 *at high elevations of Mt. Everest (PYRAMID): minimum (a), maximum (b), and mean*
 1442 *temperature (c), and precipitation (d). Uncertainty at 95% is presented as gray bar. The*
 1443 *red lines represents the robust linear fitting of the time series characterized by the*
 1444 *associated Sen's slope. According to Dytham (2011), the intercepts are calculated by*
 1445 *taking the slopes back from every observation to the origin. The intercepts used in here*
 1446 *represent the median values of the intercepts calculated for every point (Lavagnini et*
 1447 *al., 2011). For precipitation the linear fitting refers at the right axis.*

1448



1449

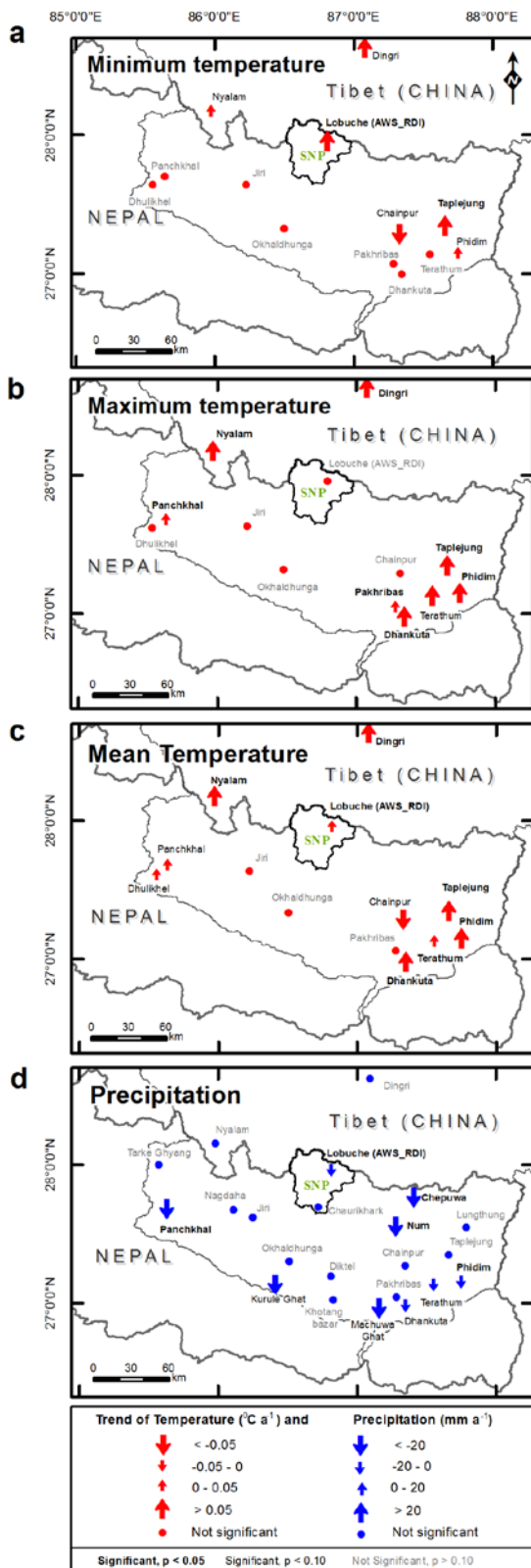
1450 *Figure 4. Trend analysis for a) minimum, b) maximum, and c) mean air temperatures*
 1451 *and d) total precipitation in the upper DK Basin. The top graph of each meteorological*
 1452 *variable shows the monthly trend (dark line) and uncertainty due to the reconstruction*
 1453 *process (gray bars). The central grid displays the results of the sequential Mann-*
 1454 *Kendall (seqMK) test applied at the monthly level. On the left, the color bar represents*
 1455 *the normalized Kendall's tau coefficient $\mu(\tau)$. The color tones below -1.96 and above*
 1456 *1.96 are significant ($\alpha = 5\%$). On the right, the monthly Sen's slopes and the relevant*
 1457 *significance levels for the 1994-2013 period ($^{\circ}$ p -value = 0.1, * p -value = 0.05, ** p -*
 1458 *value = 0.01, and *** p -value = 0.001). The bottom graph plots the progressive (black*
 1459 *line) and retrograde (dotted line) $\mu(\tau)$ applied on the annual scale. On the right, the*
 1460 *annual Sen's slope is shown for the 1994-2013 period.*



1461

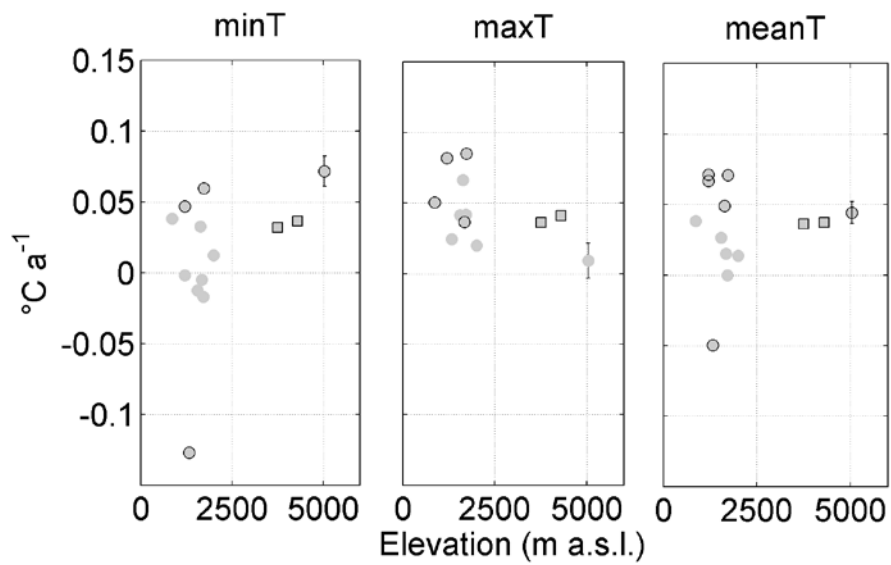
1462 | *Figure 5. Lapse rates of (a) total annual precipitation in the Koshi Basin for the last 10*
 1463 | *years (2003-2012) mean annual air temperature and (b) mean annual air temperature*
 1464 | *total annual precipitation in the Koshi Basin for the last 10 years (2003-2012). The*
 1465 | *daily missing data threshold is set to 10%. Only stations presenting at least 5 years of*
 1466 | *data (black points) are considered to create the regressions (the bars represent two*
 1467 | *standard deviations). Gray points indicate the stations presenting less than 5 years of*
 1468 | *data.*

1469



1470

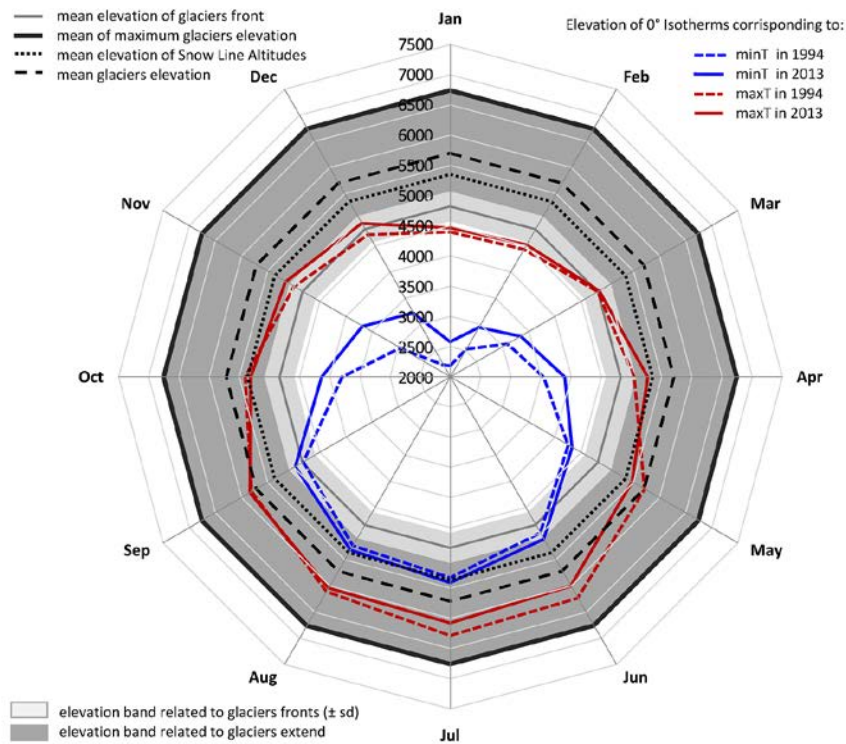
1471 *Figure 6. Spatial distribution of the Sen's slopes in the Koshi Basin for minimum (a),*
 1472 *maximum (b), and mean (c) air temperature and (d) total precipitation for the 1994-*
 1473 *2013 period. Data are reported in Table 2.*



1474

1475 *Figure 7. Elevation dependency of minimum (a), maximum (b), and mean (c) air*
 1476 *temperatures with the Sen's slopes for the 1994-2013 period. The circle indicates*
 1477 *stations with less than 10% of missing daily data, and the star indicates stations*
 1478 *showing a trend with p -value < 0.1 . The red marker represents the trend and the*
 1479 *associated uncertainty (two standard deviations) referred to the reconstructed time*
 1480 *series for the AWS1 station (Pyramid). Data are reported in Table 2.*

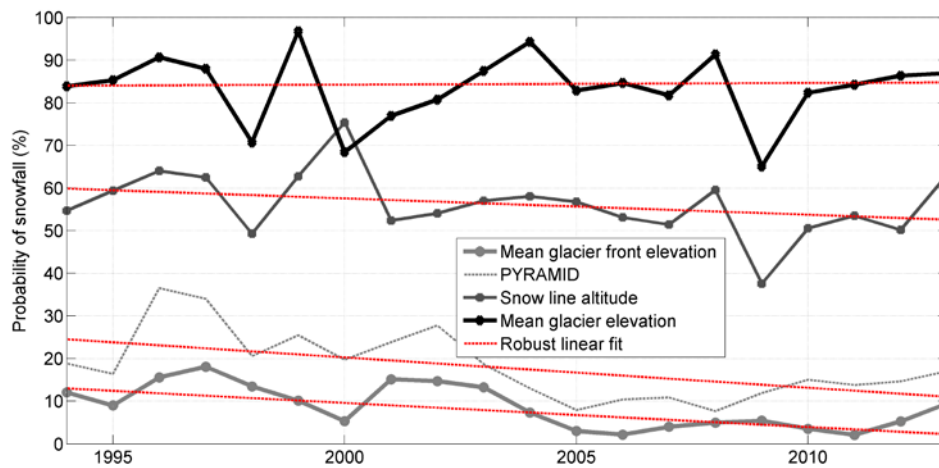
1481



1482

1483 *Figure 8. Linkage between the temperature increases and altitudinal glacier*
 1484 *distribution. The 0 °C isotherms corresponding to the mean monthly minimum and*
 1485 *maximum temperature are plotted for the 1994 and 2013 years according the observed*
 1486 *T trends and lapse rates.*

1487



1488

1489 *Figure 9. Trend analysis of annual probability of snowfall on total cumulated*
 1490 *precipitation. The red lines represents the robust linear fitting of the time series*
 1491 *characterized by the associated Sen's slope (more details in the caption of Fig. 3).*

Supplementary Material 1

Reconstruction methods of the daily temperature and precipitation time series at Pyramid station (5035 m a.s.l.)

In the following, we describe the missing daily data reconstruction performed on daily T (minimum, maximum, and mean) and Prec time series collected at Pyramid (5035 m a.s.l.) for the 1994-2013 period. As already mentioned in the main text, we consider AWS1 as the reference station (REF) for the reconstruction, which has been operating continuously from 2000 to the present. This station replaced AWS0 (1994-2005). These two stations have a recorded percentage of missing daily values of approximately 20% over the last twenty years (Table S1). The other five stations (ABC, AWSKP, AWS2, AWSN and AWS3) taken into account for the reconstruction process will be referred to as secondary stations. Information regarding the sensors used in the reconstruction process are reported in Table S2.

The time series reconstruction process considers four steps:

- 1) Pre-processing of data
- 2) Infilling method
- 3) Multiple imputation technique
- 4) Monthly aggregation of data

Step 1 – Pre-processing of data

Table 1 shows the sampling frequency of stations (ranging from 10 minutes to 2 hours). After an accurate data quality control according to Ikoma et al., 2007, a daily aggregation of the time series (temporal homogenization) is performed. Daily data have been computed only if the 100% of sub-daily data are available; otherwise, it is considered missing. These rules ensure a maximum quality of daily values with a loss of information limited to the first and last day of the failure events.

Step 2 – Infilling method

The selected daily infilling method is based on a quantile mapping regression (e.g. Déqué 2007). This method estimates a rescaling function F between two time series. This function ensures that the daily cumulated density function (cdf) of a secondary station reproduces the daily cdf of the REF over their over their common observation period. Applying the inverse function (F^{-1}) to each secondary station, a new time series is computed for each of them. In the following, these new time series with the systematic bias corrected are indicated as “*” (e.g., AWS0*, ABC*). In our case the bias is mainly due to the altitude gradient, all stations being located along the same valley (Fig. 1b).

A new time series (REF_filled) has been created merging REF and the * time series according to a priority criterion based on the degree of correlation among data (Fig. S1). The specific rules of computing are described below:

- all available data of REF are maintained in the final reconstruction without any further processing;

- the priority criterion for infilling is based on the magnitude of correlation coefficient (r) between REF and each secondary station, for each variable (Table S1); In case the daily data of the secondary station with higher r is missing the station with the slight lower r is selected.

We can observe from Table S1 that AWS0, located few tens of meters far from REF, presenting $r = 0.99$ and $r = 0.97$ for temperature and precipitation, respectively, has been the first choice. The 82% of missing daily values of temperature and 72% of precipitation are filled using the AWS0*. The second choice is ABC. Together these two stations cover more than the 90% of missing values; the whole infilling procedure allows for filling the 86% and the 91% of the overall missing values of temperature and precipitation, respectively.

Table S1. Correlation coefficients (r) between the reference station (REF) and the other secondary stations for temperature and precipitation. Furthermore the table reports the number of daily data (n) that each station has provided to the reconstruction of the time series.

Stations	Temperature		Precipitation	
	r	n	r	n
AWS0	0.99	2,144 (82.2%)	0.97	2,298 (72.2%)
ABC	0.98	254 (9.7%)	0.84	646 (20.3%)
AWSKP	0.96	48 (1.8%)	0.62	13 (0.4%)
AWS2	0.94	95 (3.6%)	0.81	145 (4.6%)
AWSN	0.92	66 (2.5%)	0.56	78 (2.5%)
AWS3	0.87	0 (0.0%)	0.53	3 (0.1%)
Total values		infilled 2,607		missing 3,183

Table S2. List of sensors with measurement height, manufacturer and accuracy. Communicated non-regular intervention as sensors or data logger replacements are reported at the table bottom.

<u>Parameter</u>	<u>Sensor</u>	<u>Manufacturer</u>	<u>Accuracy</u>
<u>AWS0⁽¹⁾</u>			
<u>Air temperature</u>	<u>Precision Linear Thermistor (2m)</u>	<u>MTX</u>	<u>0.1°C</u>
<u>Precipitation</u>	<u>Tipping Bucket (1.5m)</u>	<u>MTX</u>	<u>0.2 mm</u>
<u>Relative humidity</u>	<u>Solid state hygrometer (2m)</u>	<u>MTX</u>	<u>3%</u>
<u>Atmospheric pressure</u>	<u>Aneroid capsule (2m)</u>	<u>MTX</u>	<u>0.5hPa</u>
<u>AWS1</u>			
<u>Air temperature</u>	<u>Thermoresistance (2m)</u>	<u>Lsi-Lastem</u>	<u>0.1°C</u>
<u>Precipitation</u>	<u>Tipping Bucket (1.5m)</u>	<u>Lsi-Lastem</u>	<u>2%</u>
<u>Relative humidity</u>	<u>Capacitive Plate (2m)</u>	<u>Lsi-Lastem</u>	<u>2.5%</u>
<u>Atmospheric pressure</u>	<u>Slice of Silica (2m)</u>	<u>Lsi-Lastem</u>	<u>1hPa</u>
<u>ABC</u>			
<u>Air temperature</u>	<u>Thermoresistance (2m)</u>	<u>Vaisala</u>	<u>0.3°C</u>
<u>Precipitation</u>	<u>Acoustic (2m)</u>	<u>Vaisala</u>	<u>5%</u>
<u>Relative humidity</u>	<u>Capacitive Plate (2m)</u>	<u>Vaisala</u>	<u>3%-5%</u>
<u>Atmospheric pressure</u>	<u>Slice of Silica (2m)</u>	<u>Vaisala</u>	<u>0.5 hPa</u>
<u>AWSKP</u>			
<u>Air temperature</u>	<u>Thermoresistance (2m)</u>	<u>Lsi-Lastem</u>	<u>0.1°C</u>
<u>Precipitation</u>	<u>Tipping Bucket (1.5m)</u>	<u>Lsi-Lastem</u>	<u>1%</u>
<u>Relative humidity</u>	<u>Capacitive Plate (2m)</u>	<u>Lsi-Lastem</u>	<u>1.5%</u>
<u>Atmospheric pressure</u>	<u>Slice of Silica (2m)</u>	<u>Lsi-Lastem</u>	<u>1hPa</u>
<u>AWS2⁽²⁾</u>			
<u>Air temperature⁽³⁾</u>	<u>Thermoresistance (2m)</u>	<u>Lsi-Lastem /Vaisala</u>	<u>0.1°C/0.3°C</u>
<u>Precipitation</u>	<u>Tipping Bucket (1.5m)</u>	<u>Lsi-Lastem</u>	<u>2%</u>
<u>Relative humidity⁽³⁾</u>	<u>Capacitive Plate (2m)</u>	<u>Lsi-Lastem /Vaisala</u>	<u>1.5%/2.5%</u>
<u>Atmospheric pressure⁽³⁾</u>	<u>Slice of Silica (2m)</u>	<u>Lsi-Lastem /Vaisala</u>	<u>1hPa/0.5 hPa</u>
<u>AWSN⁽⁴⁾</u>			
<u>Air temperature</u>	<u>Thermoresistance (2m)</u>	<u>Lsi-Lastem</u>	<u>0.1°C</u>
<u>Precipitation</u>	<u>Tipping Bucket (1.5m)</u>	<u>Lsi-Lastem</u>	<u>2%</u>
<u>Relative humidity</u>	<u>Capacitive Plate (2m)</u>	<u>Lsi-Lastem</u>	<u>2.50%</u>
<u>Atmospheric pressure</u>	<u>Slice of Silica (2m)</u>	<u>Lsi-Lastem</u>	<u>1hPa</u>
<u>AWS3⁽⁵⁾</u>			
<u>Air temperature⁽⁶⁾</u>	<u>Thermoresistance (2m)</u>	<u>Lsi-Lastem /Vaisala</u>	<u>0.1°C/0.3°C</u>
<u>Precipitation</u>	<u>Tipping Bucket (1.5m)</u>	<u>Lsi-Lastem</u>	<u>2%</u>
<u>Relative humidity⁽⁶⁾</u>	<u>Capacitive Plate (2m)</u>	<u>Lsi-Lastem /Vaisala</u>	<u>1.5%/2.5%</u>
<u>Atmospheric pressure⁽⁶⁾</u>	<u>Slice of Silica (2m)</u>	<u>Lsi-Lastem /Vaisala</u>	<u>1hPa/0.5 hPa</u>

⁽¹⁾ dismissed in 2005

⁽²⁾ data logger replacement on 08/12/2010

⁽³⁾ sensors change on 05/2012 to Vaisala sensors

⁽⁴⁾ data logger replacement on 08/10/2010

⁽⁵⁾ data logger replacement on 06/10/2010

⁽⁶⁾ sensors change on 05/2013 to Vaisala sensors

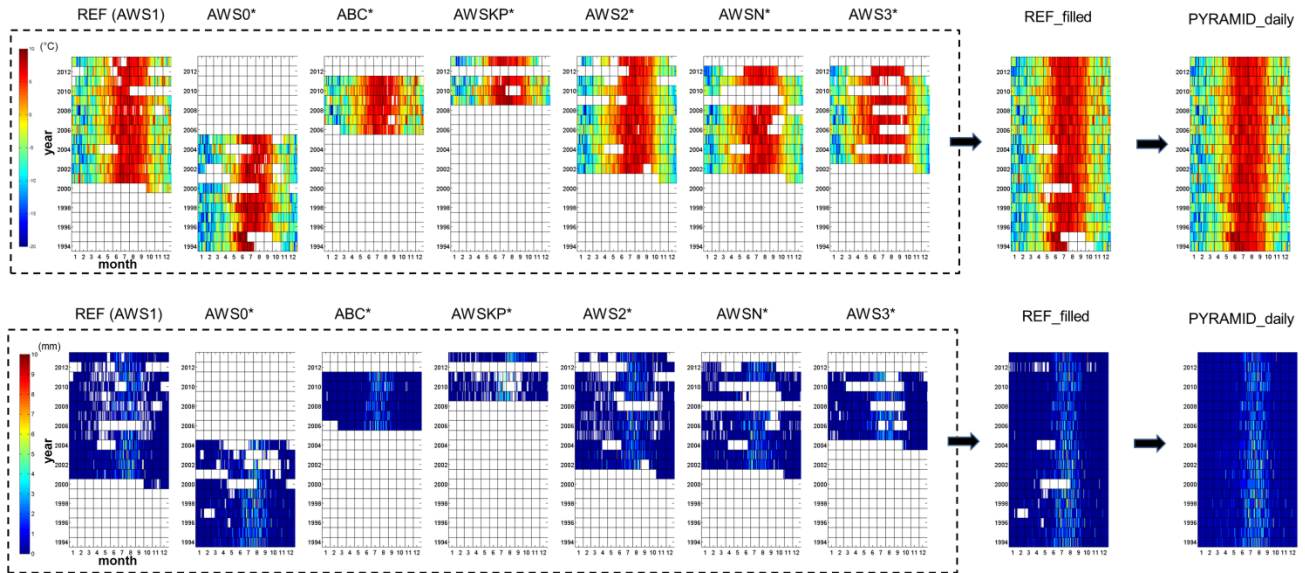


Figure S1. Scheme followed for the infilling process. Upper panel: daily mean temperature. Lower panel: precipitation. On the left, for each station, the daily data availability and the re-computed values, according to the quantile mapping procedure, are shown. On the right, a new time series (*REF_filled*) is created by merging REF (reference station) and the * time series, according to a priority criterion described in the text. In case all stations recorded some simultaneous gaps, a multiple imputation technique is applied to obtain the *PYRAMID_daily* time series.

The uncertainty associated with *REF_filled* (σ_{REF_filled}) time series derives from the quantile mapping procedure and in particular from the miss-correlation and possible non stationarity in the quantile relationship.

In order to estimate the σ_{REF_filled} , the probability distribution of the residues between REF and *time series is considered. In order to take into account the possible seasonal variability of the uncertainty, residues have been analyzed on monthly basis.

The Kolmogorov-Smirnov test (Massey, 1951), applied to distribution of the residues, verifies their normality. As a consequence, the daily uncertainty σ_{REF_filled} is estimated as the standard deviation of the residues. The estimated daily uncertainties are reported in Table [S2S3](#).

Table [S2S3](#). Daily uncertainty (expressed as °C and mm for temperature and precipitation, respectively) for each station associated with the daily data infilled through the quantile mapping regression.

Minimum Temperature (minT)												
	Jan	Feb	Mar	Apr	May	Jun	Jul	Aug	Sep	Oct	Nov	Dec
AWS0	0.95	0.98	0.72	0.65	0.49	0.48	0.29	0.35	0.49	0.77	1.09	0.86
ABC	0.82	0.79	1.6	1.29	0.9	0.58	0.66	0.45	0.56	1	0.87	0.89
AWSKP	1.41	1.3	2.25	1.62	1.54	0.84	0.84	0.71	0.65	1.29	1.18	1.61
AWS2	2.06	2.09	2.11	1.85	1.49	1.11	0.88	0.78	0.99	1.99	2.15	1.87
AWSN	2.8	2.44	1.98	1.3	1.14	0.81	0.62	0.72	0.79	1.89	2.95	2.96
AWS3	3.18	2.48	2.35	1.33	1.31	1.25	0.82	0.8	0.88	2.02	3.39	3.23

Maximum Temperature (maxT)												
	Jan	Feb	Mar	Apr	May	Jun	Jul	Aug	Sep	Oct	Nov	Dec
AWS0	0.81	0.9	0.71	1.05	0.65	0.75	0.63	0.61	0.71	1.02	0.74	1.43
ABC	0.61	0.92	1.68	1.2	1.53	1	1.07	0.65	0.75	0.77	0.65	0.62
AWSKP	1.4	1.91	2	1.58	2.12	1.31	1.02	1.07	0.8	1.21	1.49	1.35
AWS2	2.2	2.05	2.07	1.71	1.62	1.13	1.06	0.99	1.12	1.47	1.91	1.9
AWSN	3.41	3.04	2.89	2.25	2.06	1.84	1.42	1.3	1.39	2.14	3.31	3.26
AWS3	4.08	4.11	3.99	2.68	2.6	2.55	2.2	2.23	2.62	3.11	4.15	3.91

Mean Temperature (meanT)												
	Jan	Feb	Mar	Apr	May	Jun	Jul	Aug	Sep	Oct	Nov	Dec
AWS0	0.56	0.7	0.57	0.24	0.28	0.29	0.24	0.24	0.27	0.46	0.45	0.5
ABC	0.34	0.32	1.46	1.02	0.96	0.54	0.72	0.41	0.36	0.59	0.46	0.4
AWSKP	0.91	0.74	2.08	1.3	1.29	0.82	0.58	0.52	0.47	0.94	1.07	1.4
AWS2	1.8	1.88	1.71	1.38	1.1	0.66	0.5	0.43	0.57	1.56	1.88	1.53
AWSN	2.78	2.43	1.85	1.17	1.03	0.69	0.56	0.54	0.64	1.78	2.79	2.83
AWS3	3.09	2.44	2.43	1.41	1.25	1.15	0.75	0.79	1.03	1.91	3.16	3.06

Precipitation (P)												
	Jan	Feb	Mar	Apr	May	Jun	Jul	Aug	Sep	Oct	Nov	Dec
AWS0	0.68	0.22	0.43	0.99	0.61	0.72	1.34	0.93	0.61	0.29	0.38	0.04
ABC	0.02	0.03	0.07	0.28	0.52	1.17	1.91	3.42	1.49	0.1	0.19	0.04
AWSKP	0.27	0.42	0.46	1.04	0.79	1.62	2.79	2.8	1.97	2.09	0.09	0.19
AWS2	0.31	0.15	0.22	0.42	0.7	2.36	4.71	3.68	2.04	1.93	0.6	0
AWSN	0.42	0.66	0.69	1.1	1.19	2.2	5.41	5.13	3.07	1.41	0.27	0.8
AWS3	0.14	0.29	0.43	0.68	0.44	2.06	5.35	5.11	4.57	0.88	0.43	0.11

Step 3 – Multiple imputation technique

Unfortunately, all stations recorded some simultaneous gaps for a given variable: 5.7% and 4.3% for temperature and precipitation, respectively. For these cases, we applied a multiple imputation technique (the Regularized Expectation Maximization algorithm, RegEM; Schneider, 2001) to obtain the final PYRAMID_daily time series (Fig. S1).

This algorithm considers more available meteorological variables. In our case, we feed the procedure with the minimum, maximum and mean temperatures, precipitation, atmospheric pressure and relative humidity. The additional two variables (atmospheric pressure and relative humidity) allowed for a reduction of the estimated uncertainty associated with the computing of these missing data (σ_{RegEM}).

RegEM has been applied to the daily missing data on a monthly basis, considering the possible seasonal effect on the uncertainty. Table S3 reports the number of days imputed to the complete PYRAMID_daily time series for each month and for each variable. The daily standard error σ_{RegEM} estimated by the RegEM algorithm (Table S4S5) has been associated with each imputed data filled into the complete and final time series reconstructions for daily minimum, maximum, and mean temperatures and precipitation.

Table S3S4. Number of days imputed through RegEM

Variable	Jan	Feb	Mar	Apr	May	Jun	Jul	Aug	Sep	Oct	Nov	Dec
minT	0	1	1	35	87	48	68	71	60	33	10	0
maxT	0	1	1	35	87	48	68	71	60	33	10	0
meanT	0	1	1	35	87	48	68	71	60	33	10	0
Prec	13	31	14	52	99	48	31	9	1	9	4	0

Table S4S5. Uncertainty (°C and mm for temperature and precipitation, respectively) associated to the daily imputed thought RegEM

Variable	Jan	Feb	Mar	Apr	May	Jun	Jul	Ago	Sep	Oct	Nov	Dic
minT	-	3.25	2.89	2.34	2.21	1.95	0.83	0.96	1.37	2.54	2.46	-
maxT	-	3.64	3.22	2.82	2.47	1.87	1.34	1.31	1.44	2.30	2.55	-
meanT	-	3.20	2.82	2.34	2.07	1.58	0.72	0.84	1.16	2.17	2.29	-
p	0.18	0.35	0.65	0.86	0.93	2.73	4.54	4.51	2.73	1.59	0.69	-

Step 4- Monthly aggregation

Finally, the PYRAMID_daily time series, for each variable, have been aggregated on the monthly scale (hereinafter referred to as PYRAMID). The uncertainty associated with each value of the PYRAMID (named σ_m) is estimated considering the propagation of the daily uncertainty to the monthly one through the computation of the mean (for temperature) or of the sum (for precipitation).

The propagation of the uncertainty from the daily data d_i to the monthly one is different if we consider the monthly average M_m (as for temperature) or the monthly accumulation M_c (as for precipitation):

$$\sigma_m = \sqrt{\sum_{j=1}^N \left(\frac{\partial M_m}{\partial d_j} \cdot \sigma_{d_j} \right)^2} = \sqrt{\sum_{j=1}^N \left(\frac{\partial \left(\frac{1}{N} \sum_{i=1}^N d_i \right)}{\partial d_j} \cdot \sigma_{d_j} \right)^2} = \sqrt{\frac{1}{N} \sum_{j=1}^N \sigma_{d_j}^2} \quad (1)$$

$$\text{where } M_m = \frac{1}{N} \sum_{i=1}^N d_i$$

and

$$\sigma_m = \sqrt{\sum_{j=1}^N \left(\frac{\partial M_c}{\partial d_j} \cdot \sigma_{d_j} \right)^2} = \sqrt{\sum_{j=1}^N \left(\frac{\partial \sum_{i=1}^N d_i}{\partial d_j} \cdot \sigma_{d_j} \right)^2} = \sqrt{\sum_{j=1}^N \sigma_{d_j}^2} \quad (2)$$

$$\text{where } M_c = \sum_{i=1}^N d_i$$

N is the number of days of a given month and σ_{d_j} the daily uncertainty as :

$$\left\{ \begin{array}{ll} \sigma_{d_j} = 0 & \text{if the data belongs to the REF} \\ \sigma_{d_j} = \sigma_{REF_filled} & \text{if the data is imputed through infilling step} \\ \sigma_{d_j} = \sigma_{RegEM} & \text{if the data is imputed through RegEM} \end{array} \right\}$$

Finally, we estimated the uncertainty associated with the annual Sen's slopes (1994-2013) of each time series through a Monte Carlo uncertainty analysis (e.g., James and Oldenburg 1997):

- For each month value, a random realization of the normal distribution with zero-mean and σ_m standard deviation is computed.
- This uncertainty is added to each monthly estimate coming from eq. (1) or (2), obtaining a time series perturbed by the uncertainty.
- The Sen's slope and associated p-value is computed.
- The process is repeated until the convergence of the mean value of the Sen's slope and the associated standard deviation. In these regards, we observed that approximately 5000 runs are enough to ensure the convergence with a threshold of 10^{-5} °C a⁻¹ and 10^{-3} mm a⁻¹ for temperature and precipitation, respectively.

Table [S5-S6](#) reports the Sen's slopes for the 1994-2013 period calculated for each reconstructed monthly time series (PYRAMID), associated intervals of confidence (95%), median p-value and the associated [5% and 95%] quantiles.

Table [S5S6](#). Sen's slopes for the 1994-2013 period calculated for each reconstructed monthly time series (PYRAMID), associated intervals of confidence (95%), median p-value and the associated [5% and 95%] quantiles.

Time series	Sen's slope	Interval of confidence (95%)	p-value	quantiles [5% and 95%]
PYRAMID minT	0.072 °C a ⁻¹	+/- 0.011	0.0021	[0.0001-0.0212]
PYRAMID maxT	0.009 °C a ⁻¹	+/- 0.012	0.7212	[0.2843-0.9741]
PYRAMID meanT	0.044 °C a ⁻¹	+/- 0.008	0.035	[0.0053-0.1443]
PYRAMID Prec	-13.66 mm a ⁻¹	+/- 2.36	0.0021	[0.0002-0.0252]

REFERENCES

- Ikoma, E., K. Tamagawa, T. Ohta, T. Koike, and M. Kitsuregawa (2007), QUASUR: Web-based quality assurance system for CEOP reference data, *J. Meteorol. Soc. JPN.*, 85A, 461-473.
- Massey, F. J. (1951), The Kolmogorov-Smirnov Test for Goodness of Fit, *J. Am. Stat. Assoc.*, 46(253), 68-78.

Supplementary Material 2

Further analysis on the non-stationarity of the reconstructed daily precipitation time series at Pyramid station

The analysis described in the following aims at assessing whether the decreasing trend of precipitation observed for the daily time series reconstructed at Pyramid (1994-2013) is due to a reduction of duration or to a reduction of intensity.

To this goal we considered two different periods p , say $p1 = 1994-1998$ and $p2 = 2009-2013$, which correspond to the first and last five years of the whole analysis period $p0 = 1994-2013$. For a given week w , the mean weekly-cumulated precipitation RR_w^p is defined as $RR_w^p = (\sum_{y=1}^N RR_{w,y})/N$, where N is the number of years during the period p .

The difference between the mean weekly-cumulated precipitation RR_w^{p1} and RR_w^{p2} may be attributed to a change in the corresponding duration and/or intensity. To separate the relative contributions, we defined two descriptors:

1-The duration of precipitation for a given week w of the year y is described by the number of wet days $W_{w,y}$, where a “wet day” is defined by the threshold $RR > 1$ mm. Then, the mean W_w^p over a given period p of N years is computed as:

$$W_w^p = \frac{1}{N} \sum_{y=1}^N W_{w,y} \quad (1)$$

2- The daily intensity of precipitation for a given week w of the year y is computed as the cumulative precipitation $RR_{w,y}$ divided by the number of wet days $W_{w,y}$. Then, a mean intensity index $SDII_w^p$ over a given period p of N years is computed as:

$$SDII_w^p = \frac{1}{N} \sum_{y=1}^N \frac{RR_{w,y}}{W_{w,y}} \quad (2)$$

An attempt to quantify the contribution to the variation in precipitation arising from variation in duration and/or intensity is to consider one of the two terms stationary over the whole period. This is a rough approximation as the non-stationarity may not be linear. However, an estimation of the relative contribution arising from the change in duration can be expressed considering the intensity of precipitation as stationary over the whole period $p0$ ($SDII_w^{p0}$) and computing the variation of precipitation due only to a variation in duration, i.e. $(W_w^{p2} - W_w^{p1}) * SDII_w^{p0}$. The relative contribution RLD to the total change $(RR_w^{p2} - RR_w^{p1})$ can be estimated as:

$$RLD = \frac{(W_w^{p2} - W_w^{p1}) * SDII_w^{p0}}{(RR_w^{p2} - RR_w^{p1})} * 100 \quad (3)$$

The indexes proposed above are shown in figure S6 in dark blue area for the 1994-1998 period and light blue area for the 2009-2013 period for the W_w^p , $SDII_w^p$ and RR_w^p (panel a, b and c respectively). For each index, we defined as residues the difference between the two periods (red bar plot).

The RLD (shown in red on the right axis of the panel c) indicates that the early and late monsoon are more affected by the reduction in duration than intensity, while it is the opposite during the monsoon.

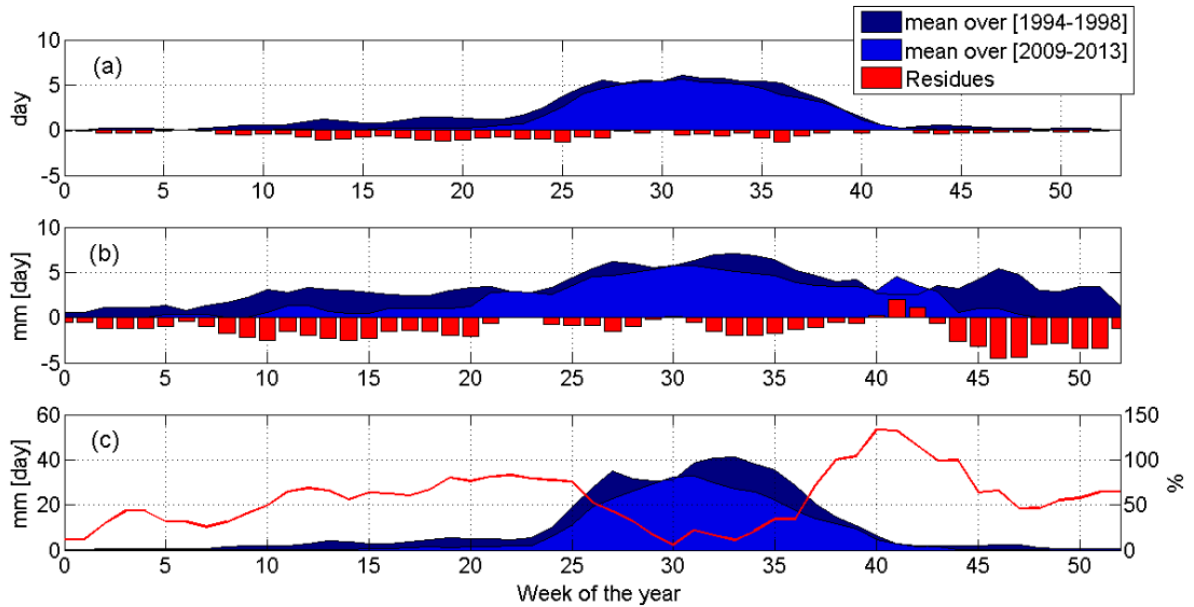


Figure S6. Panel a: Mean number of wet day per week W_w^p . Panel b: Mean daily precipitation intensity $SDII_w^p$ (mm). Panel c: Mean weekly-cumulated precipitation RR_w^p and relative contribution of the change in duration RLD in % (red line)

Supplementary Material 3

Evaluation of the possible underestimation of solid precipitation at Pyramid

The Chaurikhark station (ID 1202) (Fig. 1b, Table 2) is located at 2619 m a.s.l., along the same valley of PYRAMID (Dud Koshi). This station records only daily precipitation with a tipping bucket. Not having the availability of air temperature data, we estimated for this location the mean daily values for the 1994-2013 period through of the lapse rate and the mean daily air temperature series reconstructed in this study at PYRAMID.

The precipitation phase has been taken into account assuming that the probability of snowfall and rainfall depends on the mean daily air temperature (as well as we did for PYRAMID, see the text). In Figure S7 we observe that 86% of precipitation is concentrated during June-September. The probability of snowfall is very low (0.6%) and it is completely concentrated in December, January, and February (the mean temperature of these months is about 5 °C).

We realized the scatter-plot of Figure S8 between their monthly precipitation (averaged on 1994-2013 period) in order to compare the two stations. Data were previously log transformed assuring their normal distribution. First of all, we observe the strong relationship due to the fact that they belong to the same valley, although there are 2400 m of altitudinal range. Secondly, we note the variability between the two stations is higher for those months which record less precipitation (spring and winter). Probably, during these months, PYRAMID underestimates the solid precipitation which fall in liquid form at lower elevation (Chaurikhark). In this regard we realized the graph of Figure S8 for showing the precipitation ratio between PYRAMID and Chaurikhark. We observe that during the monsoon (June-September), period of the year when the probability of snowfall at PYRAMID is very low (4%) (see the text), the precipitation ratio is $21\pm 3\%$ (standard deviation) that means at 5050 m a.s.l. it rains a fifth respect to 2600 m a.s.l. (see Fig. 5). Outside the monsoon months this ratio decreases to $15\pm 6\%$. Assuming that this lower ratio if completely attributable to the solid precipitation not captured at high elevations, we calculated an underestimation of $15\pm 5 \text{ mm y}^{-1}$, corresponding to $3\pm 1\%$ of the total annual cumulated precipitation at PYRAMID (446 mm y^{-1}).

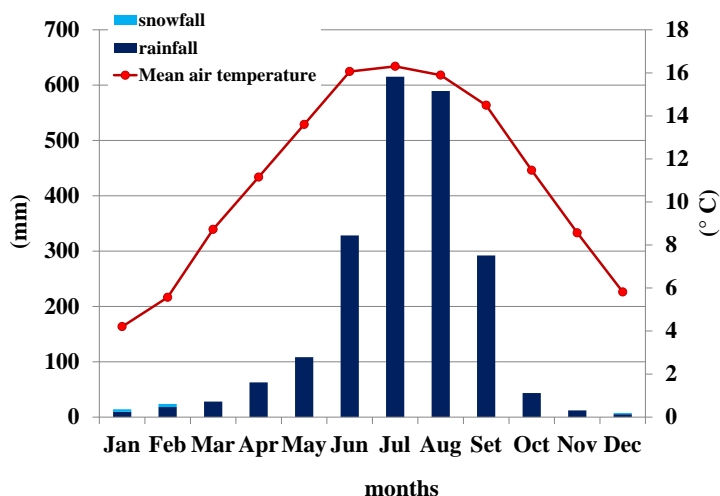


Figure S7. Mean monthly cumulated precipitation subdivided into snowfall and rainfall and mean temperature at Chaurikhark station (ID 1202) (reference period 1994-2013). The bars represent the standard deviation.

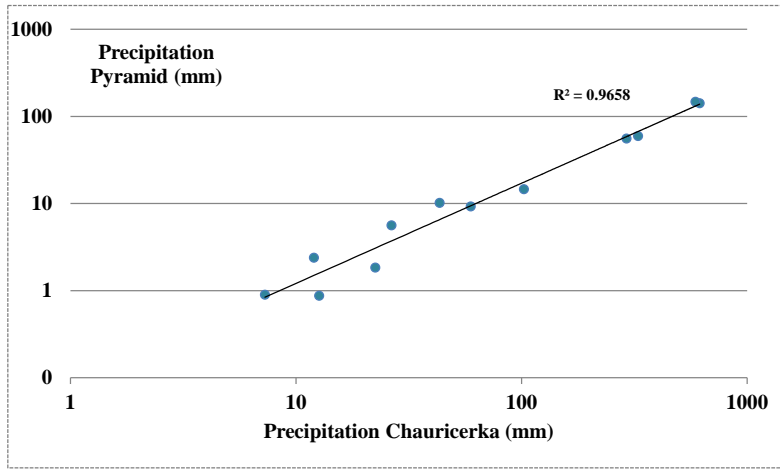


Figure S8. Scatter-plot between the monthly precipitation of PYRAMID and Chaurikhark (averaged on 1994-2013 period).

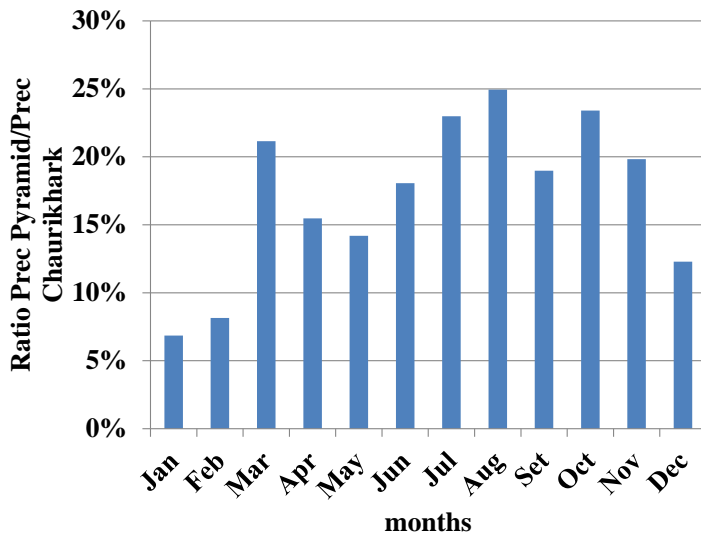


Figure S9. Ratio between the PYRAMID and Chaurikhark total precipitation for each month (averaged on 1994-2013 period).